Delft University of Technology

Document Version
Final published version

Licence
CC BY

Citation (APA)
Li, Y., Rietveld, L. C., & Heijman, S. G. J. (2026). Analysis of fouling control strategies in ceramic nanofiltration membranes: $CaCO_3$ precoating versus continuous dosing. *Desalination*, *637*, Article 120502. https://doi.org/10.1016/j.desal.2026.120502

Important note
To cite this publication, please use the final published version (if applicable).
Please check the document version above.

Copyright
In case the licence states “Dutch Copyright Act (Article 25fa)”, this publication was made available Green Open Access via the TU Delft Institutional Repository pursuant to Dutch Copyright Act (Article 25fa, the Taverne amendment). This provision does not affect copyright ownership.
Unless copyright is transferred by contract or statute, it remains with the copyright holder.

Sharing and reuse
Other than for strictly personal use, it is not permitted to download, forward or distribute the text or part of it, without the consent of the author(s) and/or copyright holder(s), unless the work is under an open content license such as Creative Commons.

Takedown policy
Please contact us and provide details if you believe this document breaches copyrights.
We will remove access to the work immediately and investigate your claim.

This work is downloaded from Delft University of Technology.

Desalination 637 (2026) 120502

Contents lists available at ScienceDirect

Desalination

journal homepage: www.elsevier.com/locate/desal

Analysis of fouling control strategies in ceramic nanofiltration membranes: $CaCO_3$ precoating versus continuous dosing

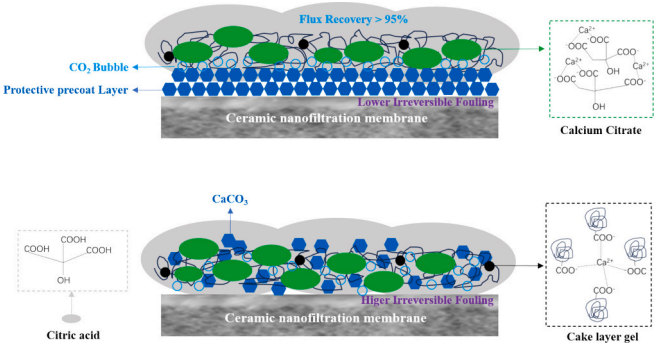
Yuke Li [a,*], Luuk C. Rietveld [a], Sebastiaan G.J. Heijman [a]

[a] Section of Sanitary Engineering, Department of Water Management, Faculty of Civil Engineering and Geosciences, Delft University of Technology, Stevinweg 1, 2628 CN, Delft, the Netherlands

HIGHLIGHTS

- Precoating ceramic NF membranes achieved 95% permeability recovery vs 82% for continuous dosing after 1st cleaning cycle
- Precoated membranes exhibited substantially lower irreversible fouling compared to continuously dosed and uncoated membranes
- Precoating formed a stratified protective barrier; continuous dosing produced a mixed organic-inorganic composite layer
- Precoated membranes achieved 94% DOC removal, and >98% rejection of F^- and PO_4^{3-}

GRAPHICAL ABSTRACT



ARTICLE INFO

Keywords:
Ceramic membranes
Nanofiltration
Continuous dosing
Membrane fouling control
$CaCO_3$ precoating
Permeability recovery

ABSTRACT

Ceramic membrane filtration is increasingly applied in water reclamation and purification, demonstrating particular efficacy in treating challenging industrial wastewater streams and non-potable water sources. During precoating, a removable filtration layer can be deposited on the membranes to enhance particle retention and reduce fouling, although it requires periodic renewal. The continuous dosing strategy is implemented by premixing calcium carbonate ($CaCO_3$) with the feed solution at the onset of each cycle, prior to the start of filtration. Both methods address membrane fouling but differ fundamentally in longevity and modification mechanisms. In this study, dead-end filtration was employed to deposit a $CaCO_3$ coating, with particular focus on fouling mitigation using citric acid treatment. Compared to the precoating method, the continuous dosing method enabled the addition of $CaCO_3$ throughout the fouling experiment, followed by citric acid cleaning. Experimental results demonstrated that, although the continuous dosing method also showed good permeability recovery, the precoated membrane exhibited better permeability recovery than the continuous dosing method, with consistent observations across both model wastewater and surface water. This performance difference likely results from

Abbreviations: Al_2O_3, aluminum oxide/alumina; $CaCO_3$, calcium carbonate; $CaCl_2$, calcium chloride; CO_2, carbon dioxide; CaF_2, fluorite; $Ca_5(PO_4)_3OH$, hydroxyapatite; DOC, dissolved organic carbon; EDS, energy-dispersive X-ray spectroscopy; 3D-EEM, three-dimensional excitation-emission matrix; Em, emission wavelength; Ex, excitation wavelength; HCl, hydrochloric acid; IC, ion chromatography; MF, microfiltration; MWCO, molecular weight cutoff; NaCl, sodium chloride; $NaHCO_3$, sodium bicarbonate; NF, nanofiltration; NOM, natural organic matter; PEG, polyethylene glycol; SD, standard deviation; SEM, scanning electron microscopy; TiO_2, titanium dioxide; TMP, transmembrane pressure; TOC, total organic carbon; UF, ultrafiltration; XRD, X-ray diffraction; ZrO_2, zirconium dioxide.

* Corresponding author.
E-mail addresses: yukeli94@163.com, L.Li-6@tudelft.nl (Y. Li).

https://doi.org/10.1016/j.desal.2026.120502
Received 28 May 2026; Received in revised form 26 June 2026; Accepted 1 July 2026
Available online 2 July 2026
0011-9164/© 2026 The Author(s). Published by Elsevier B.V. This is an open access article under the CC BY license (http://creativecommons.org/licenses/by/4.0/).

the protective $CaCO_3$ layer on the membrane, while the continuous dosing method allowed for partial foulant deposition before sufficient $CaCO_3$ coverage was achieved. The precoated membrane exhibited the lowest irreversible fouling (3×10^{10} m^{-1} after the second cycle, versus 21×10^{10} m^{-1} for continuous dosing and 72×10^{10} m^{-1} for the uncoated membrane). The precoated membrane also performed better in treating Schie Canal water. The treatment system showed better performance in bulk water quality improvement, achieving a 94% removal of dissolved organic carbon and a 65% reduction in electrical conductivity. The process exhibited high ion selectivity, rejecting divalent cations (Ca^{2+}, Mg^{2+} > 68%) and specific anions, with particularly high removal rates for fluoride and phosphate (F^-, PO_4^{3-} > 98%).

1. Introduction

Ceramic membrane filtration is increasingly regarded as a promising water treatment technology, particularly in industrial applications [1,2]. These membranes typically feature an asymmetric architecture with multiple layers, including a porous support substrate and a thin selective top layer [3]. The composite structure is fabricated using various metal oxides - while aluminum oxide (Al_2O_3) primarily forms the support layer, the separation layer is often composed of titanium dioxide (TiO_2) or zirconium dioxide (ZrO_2) coatings [4–6]. Unlike polymeric alternatives, ceramic membranes exhibit a uniform surface chemistry characterized by abundant metal hydroxyl groups, resulting in significantly enhanced surface hydrophilicity [7,8]. This characteristic is important for mitigating organic fouling [9]. Previous studies have explored various metal oxide modifications to enhance membrane performance through either increased electrostatic repulsion or steric hindrance effects against organic contaminants [10]. Such surface engineering strategies can also effectively minimize the deposition of charged organic compounds on membrane surfaces, thereby substantially reducing fouling tendencies [11,12].

The operational efficacy of membrane systems is still compromised by fouling phenomena, resulting in an elevated transmembrane pressure (TMP) and, in severe cases, deterioration of permeate quality [13]. These fouling-induced effects require increased maintenance interventions, ultimately impacting both production capacity and economic viability of water treatment facilities [14,15]. Four dominant types of fouling can be identified [16,17]: particulate deposition (physical blockage), organic/inorganic scaling (including gel-layer formation), biofouling (microbial colonization), and chemical precipitation (scaling reactions). In addition, organic compounds and colloidal particles can demonstrate synergistic fouling through gel-layer formation, while biodegradable compounds can promote biofilm development [17]. Recent technological advancements in fouling mitigation have focused on three principal approaches: surface property modification (hydrophilicity enhancement and/or charge increase), nanocomposite integration (through blending or surface deposition) and dynamic filtration aids (precoat applications) [18]. Precoating has emerged as an effective fouling control approach for various membrane processes, including polymeric and ceramic microfiltration (MF), ultrafiltration (UF), and membrane distillation systems [18–20]. This technique involves the deposition of a permeable, removable layer onto the membrane surface prior to filtration. During operation, foulants primarily accumulate on the precoat layer, which can subsequently be removed via hydraulic backwashing, thereby restoring membrane performance [21]. As an example, coagulant-based precoating using iron or aluminum salts has been employed to enhance natural organic matter (NOM) removal by forming flocs that are eliminated during backwashing in ceramic MF/UF applications [22,23].

Unlike MF/UF membranes, ceramic NF modules are susceptible to structural damage under high-pressure backwashing conditions, primarily due to mechanical stress on the membrane seals, while low-pressure backwashing has proven to be ineffective for the removal of membrane fouling [24]. Consequently, chemical cleaning remains the predominant fouling control method for ceramic NF [5,25].

The precoating technique involves the deposition of a preformed filtration layer onto the membrane substrate prior to the filtration process [26]. This auxiliary layer, typically composed of particulate materials, functions as a secondary filtration barrier that enhances particulate retention efficacy while mitigating direct membrane fouling [27,28]. As a non-permanent modification, the precoat layer requires periodic replenishment due to operational degradation and saturation effects during filtration cycles. Recent studies have explored calcium carbonate ($CaCO_3$) precoating on tubular ceramic NF membranes combined with acid-assisted forward flushing, demonstrating its potential for fouling mitigation [24,29]. In addition, it has been demonstrated that $CaCO_3$ pre-deposition considerably enhances the antifouling performance of ceramic NF membranes [18]. Unlike sacrificial precoating, continuous dosing incorporates the coating into the fouling layer while preserving the membrane's baseline permeability. This approach enhances selectivity and antifouling properties without requiring recurrent coating procedures. The continuous dosing method could also operate by dosing a $CaCO_3$ coating agent in the fouling solution, enabling acid-mediated reactions that directly dissolve membrane surface blockages. However, a comparison between precoating and continuous dosing (i.e., premixing $CaCO_3$ with the foulant solution for the whole filtration) has not been reported. The mechanistic understanding of why precoating achieves better cleaning efficacy despite lower $CaCO_3$ consumption remains incomplete. Also, the potential of the $CaCO_3$ precoat to enhance the rejection of specific contaminants (e.g., fluoride and phosphate) has not been explored. Our study aims to (I) quantitatively compare the fouling control performance of $CaCO_3$ precoating versus continuous dosing under identical conditions; (II) propose a bubble-location-based mechanism to explain the observed differences; and (III) evaluate the multifunctional rejection performance of the precoated membrane for both organic and ionic contaminants.

2. Methods and materials

2.1. Ceramic membranes properties

This study incorporated a ceramic nanofiltration membrane. It was procured from a commercial supplier (Inopor GmbH, Germany), featuring a dual-layer architecture comprising an α-alumina (α-Al_2O_3) support substrate and a titanium dioxide (TiO_2) selective layer [24]. These monolithic multichannel modules contained 19 parallel flow channels, each with 3.5 mm internal diameter, spanning 0.5 m in length, yielding a total effective filtration area of 0.1045 m^2. According to the manufacturer's specifications, the membranes exhibited [30]:

- Nominal molecular weight cutoff (MWCO): 450 *Da*
- Porosity range: 30–40%
- Mean pore diameter: 0.9 nm

The MWCO of the membrane was determined by a systematic approach, as documented by Caltran et al. and Shang et al. [30,31]. This method employs polyethylene glycol (PEG) standards of varying molecular weights (200–1000 *Da*), sourced from Sigma-Aldrich, Germany. Following this protocol, the membrane used in this study was tested. The analysis of PEG was carried out with a Shimadzu Prominence HPSEC system from Japan, which was fitted with a 5 mm, 30 Å gel permeation

column from PSS GmbH, Germany, and a Shimadzu RID-20A refractive index detector [32].

2.2. Synthesis of $CaCO_3$ nanoparticles

A study on $CaCO_3$ particle size effects on fouling mitigation was conducted using both synthesized and commercially obtained materials, where nanoscale $CaCO_3$ particles were generated through chemical precipitation by reacting calcium chloride ($CaCl_2$) with sodium bicarbonate ($NaHCO_3$). Electrokinetic potential measurements were performed using Malvern Zetasizer. Colloidal stability optimization was achieved through zeta potential enhancement by introducing excess Ca^{2+} into the aqueous suspension, with ionic concentrations of 9 mM for Ca^{2+} and 3 mM for bicarbonate (HCO_3^-) to adjust surface charge characteristics and prevent particle reaggregation [24]. The particle size distribution of the synthesized $CaCO_3$ suspension was characterized by dynamic light scattering. As summarized in Table S1, the suspension exhibited a D50 of 0.192 μm and a D10 of 0.175 μm, and a D90 of 0.429 μm, with a span value of 1.32 calculated as (D90 − D10) / D50, indicating a relatively narrow distribution. The polydispersity index (PDI) was approximately 0.28. The main peak was centered at 0.187 μm, accounting for 34.5% of the total particle volume, with minor secondary peaks observed at 0.172 μm (4.2%) and 0.223 μm (3.5%). More than 99% of the particles were smaller than 0.243 μm, confirming the absence of large aggregates. The zeta potential of the suspension was measured as +24.8 mV, indicating good colloidal stability. These particle size characteristics remained stable over the course of the fouling experiments (within 24 h), ensuring the reproducibility of the precoating process. This deposition was conducted under a TMP of 8–10 bar and a permeate flux of 100–120 $L{\cdot}m^{-2}{\cdot}h^{-1}$ for 5–10 min, aiming to achieve a uniform coating distribution across the filtration surface.

2.3. Feed water (model sewage and surface water)

Sodium alginate, a representative gel-forming foulant frequently employed in membrane fouling studies [33], was used to simulate organic fouling through gel layer formation on membrane surfaces. The synthetic wastewater contained 0.4 $g{\cdot}L^{-1}$ sodium alginate (Sigma-Aldrich) with a supporting electrolyte, including 1 mM $NaHCO_3$ (buffer, for pH stabilization at 7.5), 5 mM NaCl (ionic strength adjustment), and 3 mM $CaCl_2$. Ca^{2+} ions were included because they interact with carboxyl functional groups on alginate polymers, facilitating intermolecular crosslinking that establishes the characteristic “egg-box” configuration, recognized as a fundamental fouling mechanism [34]. According to Kramer et al. [35], experimental studies on real wastewater filtration reveal a 58% decline in membrane permeability after five days of operation, indicating significant fouling of the ceramic NF membrane. To accelerate fouling under controlled conditions, a high concentration of sodium alginate was employed, enabling substantial membrane fouling within only 40 min of filtration—a duration equivalent to approximately five days of typical operation with raw sewage [29].

To compare the fouling with sodium alginate-based synthetic wastewater with surface water fouling, surface water from the Schie Canal was employed as feedwater. Surface water represented natural systems, containing complex foulants like natural organic matter, microorganisms, particles and salts, which led to combined fouling mechanisms [36]. Synthetic wastewater with sodium alginate, a model polysaccharide, simulated organic/gel-layer fouling, allowing for isolation of specific interactions, e.g. with calcium ions (Ca^{2+}) [37,38].

The concentration of dissolved organic carbon (DOC) was evaluated with a Shimadzu TOC VPH analyzer. This instrument employs oxidative combustion coupled with infrared detection, a method recognized as a global standard for DOC quantification [39]. Ionic constituents (including inorganic species and low-molecular-weight organic ions) were resolved and quantified via suppressed conductivity ion chromatography (IC) employing an ion-exchange resin stationary phase, where separation occurs through differential ionic affinities [40]. All chromatographic data were acquired and processed using MagIC Net software.

2.4. Filtration set-up

The study employed a continuous-flow, constant flux, membrane system operating under controlled hydrodynamic conditions, using a dual-pump configuration, comprising a feed pressure pump and a cross-flow circulation pump to maintain constant permeate flux and cross-flow velocity throughout the experimental runs (Fig. 1). Seven feed solutions were used in the filtration experiments: (i) Deionized water, for baseline permeability measurement and post-cleaning rinsing; (ii) $CaCO_3$ suspension, to form a precoating layer; (iii) Synthetic wastewater (sodium alginate), as a model organic foulant; (iv) Synthetic wastewater with $CaCO_3$, to compare with the precoat method; (v) Surface water (Schie Canal water), representing natural foulants; (vi) Schie Canal water with $CaCO_3$, to evaluate combined fouling effects; (vii) Citric acid solution, for chemical cleaning between trials. The experimental protocol consisted of a fixed permeate flux of 20 $L{\cdot}m^{-2}{\cdot}h^{-1}$ for model sewage and 40 $L{\cdot}m^{-2}{\cdot}h^{-1}$ for Schie canal water, and a cross-flow velocity of 0.67 $m{\cdot}s^{-1}$ to ensure a turbulent flow regime within the tubular NF membrane configuration, while allowing the TMP to fluctuate between 1 and 10 bar in response to fouling development and cleaning efficacy [34]. All feed solutions, except ultrapure water, were continuously recirculated through the system's feed reservoir (Fig. 1) to maintain consistent solution characteristics throughout each experimental phase. The flux values employed in this study (20–40 $L{\cdot}m^{-2}{\cdot}h^{-1}$) were selected to accelerate fouling for comparative evaluation within practical experimental durations. In full-scale applications, lower fluxes (e.g., 5–10 $L{\cdot}m^{-2}{\cdot}h^{-1}$) are typically used, under which the fouling rate would be slower [41]; however, the relative performance advantage of the precoating strategy over continuous dosing is expected to persist across different flux conditions. The relative performance advantage of precoating over continuous dosing observed at accelerated fluxes may not directly translate to full-scale conditions; validation at typical operational fluxes is needed to confirm practical applicability.

The membrane permeability under fouling conditions was calculated using temperature-corrected values (Eq. (1)) [38] to account for minor variations in ambient temperature that could affect fluid viscosity and system performance during experimental testing.

$$L_{20^oC} = \frac{J \bullet e^{-0.0239\bullet(T-20)}}{\Delta P} \tag{1}$$

where L represents the temperature-compensated membrane permeability expressed in liters per square meter per hour per bar ($L{\cdot}m^{-2}{\cdot}h^{-1}{\cdot}bar^{-1}$), T denotes the measured water temperature in degrees Celsius (°C), J corresponds to the volumetric flux through the membrane in liters per square meter per hour ($L{\cdot}m^{-2}{\cdot}h^{-1}$), and ΔP represents the TMP expressed in bars, calculated as the arithmetic mean of pressure measurements obtained from the feed and concentrate streams.

The efficacy of membrane cleaning protocols was quantitatively evaluated through a permeability restoration analysis, with the degree of recovery being calculated using the established mathematical relationship presented in Eq. (2) [2]. Eq. (2) defines the permeability recovery ratio as the fraction of the lost permeability (relative to the first-cycle decline) that is restored after cleaning in a subsequent cycle. The first-cycle permeability decline is chosen as the normalization reference because it represents the maximum fouling-induced loss under the given conditions and establishes a consistent baseline for evaluating the cleaning effectiveness across cycles. This normalization allows direct comparison of cleaning performance between different fouling control strategies, even when the absolute permeability losses differ.

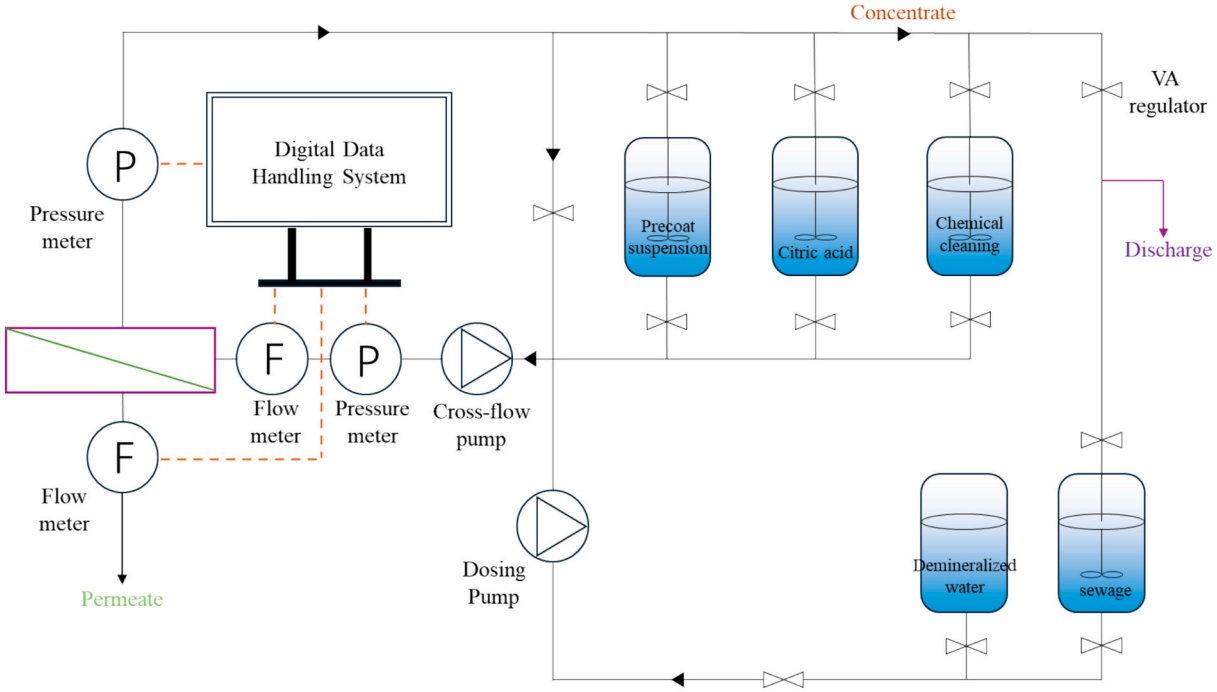


Fig. 1. Schematic of the cross-flow ceramic nanofiltration [42] bench-scale setup.

$$\textit{Permeability recovery} = \frac{L_{i,0} - L_{1,e}}{L_{1,0} - L_{1,e}} \tag{2}$$

where $L_{1,0}$ denotes the baseline permeability ($L{\cdot}m^{-2}{\cdot}h^{-1}{\cdot}bar^{-1}$) measured at the start of the first operational cycle; $L_{1,e}$ represents the terminal permeability ($L{\cdot}m^{-2}{\cdot}h^{-1}{\cdot}bar^{-1}$) recorded at the end of the first cycle; $L_{i,0}$ indicates the initial permeability ($L{\cdot}m^{-2}{\cdot}h^{-1}{\cdot}bar^{-1}$) for any given subsequent cycle i; and $L_{i,e}$ corresponds to the final permeability ($L{\cdot}m^{-2}{\cdot}h^{-1}{\cdot}bar^{-1}$) achieved upon completion of cycle i.

To evaluate permeability restoration dynamics, the normalized permeability (L_1/L_0) was computed, with L_1 ($L{\cdot}m^{-2}{\cdot}h^{-1}{\cdot}bar^{-1}$) represents the permeability under current conditions and L_0 ($L{\cdot}m^{-2}{\cdot}h^{-1}{\cdot}bar^{-1}$) represents the clean water permeance at experiment initiation. Three critical permeability measurements were conducted: (1) uncoated membrane characterization prior to fouling experiments, (2) post-$CaCO_3$ precoating analysis to determine coating-induced permeance decline, and (3) post-fouling/cleaning evaluation using deionized water to assess cleaning efficacy. Membrane fouling progression was quantified through calculation of the fouling resistance parameter (Eq. (3)) [43–45]:

$$J_m = \frac{\triangle P_m}{\mu R_t} = \frac{\triangle P_m}{\mu(R_i + R_r + R_{ir})} \tag{3}$$

where J_m ($m{\cdot}s^{-1}$) characterizes transmembrane flux, μ (Pa·s) represents permeate viscosity, R_t indicates total fouling, R_i intrinsic membrane fouling, R_r reversible fouling, and R_{ir} irreversible fouling.

All filtration and characterization experiments described in the following sections were performed in duplicate to ensure reproducibility. Data are expressed as mean ± standard deviation (SD). Error bars in all figures represent the SD calculated from two independent measurements ($n = 2$), unless otherwise specified.

2.5. Application of the $CaCO_3$ precoat and continuous dosing

Deposition of $CaCO_3$ for precoating was achieved through dead-end filtration of the precoat solution at pressures ranging between 8 and 10 bar, corresponding to fluxes of 90–110 $L{\cdot}m^{-2}{\cdot}h^{-1}$, which facilitated membrane surface coverage [2]. To determine the optimal $CaCO_3$ loading, a series of preliminary experiments were conducted with loadings ranging from 5 to 20 $g{\cdot}m^{-2}$ [29]. The optimal loading was selected based on the criterion of achieving the highest permeability recovery while maintaining an acceptable initial permeability loss (<30%). Preliminary tests with lower loadings (<11.5 $g{\cdot}m^{-2}$) showed incomplete membrane coverage and lower recovery (<70% after cleaning), whereas higher loadings (>11.5 $g{\cdot}m^{-2}$) caused excessive initial flux loss (>35%) without further improving cleaning efficiency. Thus, a loading of 11.5 $g{\cdot}m^{-2}$ (equivalent to 1200 mg per membrane module) was chosen as optimal. Long-term fouling resistance and cleaning frequency were not used as optimization criteria in this study, as the primary goal was to compare precoating and continuous dosing strategies under standardized conditions. The $CaCO_3$ precoat layer applied in this study was physically deposited on the membrane surface via dead-end filtration, forming a loose deposited layer without chemical bonding or strong adhesion. Experimental validation showed that under a cross-flow velocity of 0.67 $m{\cdot}s^{-1}$ (corresponding to a Reynolds number of 2329), the precoat layer remained intact during the filtration experiments without being washed off, as evidenced by the fact that the membrane permeability remained consistent before and after cross-flow rinsing. In tubular membranes, even under turbulent flow conditions, a viscous sublayer (stagnant layer) exists near the membrane surface, where the flow velocity is extremely low. According to the stagnant layer thickness estimation formula [46,47], the calculated thickness of the stagnant layer is approximately 32.9 μm. In this study, the thickness of the $CaCO_3$ precoat layer was only 7–9 μm, which lies well within the stagnant layer. The flow velocity within the stagnant layer is less than 1% of that in the bulk flow region [48]. Consequently, the shear force acting on the $CaCO_3$ particles is extremely small, insufficient to cause particle detachment or mechanical wear on the membrane surface. The protocol for the continuous dosing experiment (Fig. 2) involved the addition of $CaCO_3$, with each dosage (400 mg per cycle) compensating for the equivalent of one filtration cycle of the precoated membrane. The term “continuous dosing” refers to the strategy in which $CaCO_3$ is added to the feed water at the beginning of each operational cycle and remains present throughout the entire filtration cycle, rather than being injected incrementally or metered continuously in real time during operation.

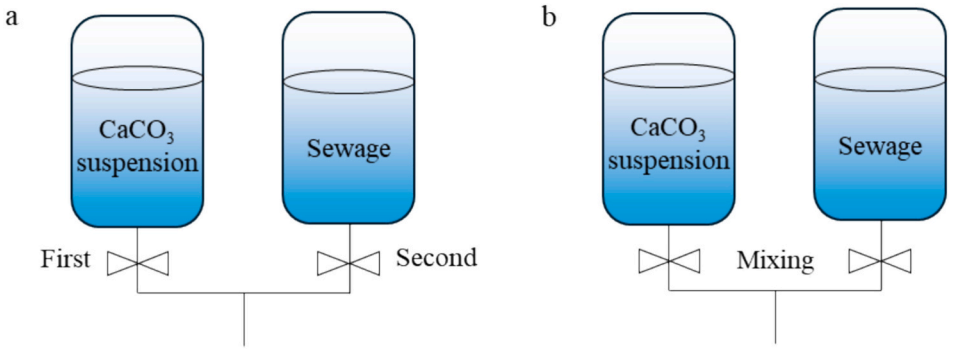


Fig. 2. Diagram for the process of (a) precoat and (b) continuous dosing.

This mode is equivalent to a cyclic co-dosing approach, where a defined amount of $CaCO_3$ (400 mg per cycle) is replenished at the start of each cycle. In the continuous dosing strategy, $CaCO_3$ is continuously available in the feed during each cycle, providing sustained reactivity with citric acid for cleaning.

Following the fouling process, acid cleaning was performed using citric acid. The interaction between this acid and the $CaCO_3$ is described by Eq. (4):

$$CaCO_3(s) + C_6H_8O_7(aq) \rightarrow Ca^{2+}(aq) + C_6H_6O_7^{2-}(aq) + H_2O(l) + CO_2(g) \quad (4)$$

The initial permeability of the ceramic membrane was determined using demineralized water. In the experiments involving the precoated membrane, a layer of $CaCO_3$ was first applied to the membrane surface under pressure. Subsequently, a model wastewater based on sodium alginate solution was filtered to simulate the fouling process. Following fouling, citric acid was introduced to react with the precoat layer, yielding acidic reaction products and carbon dioxide. The final step involved a 10-minute forward flush at a velocity of 0.67 $m{\cdot}s^{-1}$, which removed a portion of the fouling layer. In the comparative continuous dosing experiment, $CaCO_3$ was initially introduced into the feed water and thoroughly mixed prior to initiating filtration. Following fouling formation, citric acid was introduced to react with $CaCO_3$ within the fouling layer, producing acidic byproducts and carbon dioxide. The process concluded with a 10-minute forward flush at 0.67 $m{\cdot}s^{-1}$ to partially remove the fouling layer. All filtration experiments with 3 cycles (40 min of model sewage and 6 h of Schie Canal water) were duplicated [49], to confirm the reproducibility and feasibility [50]. A digital microscope equipped with a built-in LED light source was employed to observe the membrane surface during both the precoating and continuous dosing phases. The observations revealed two distinct states of the acid reaction.

2.6. Chemical cleaning

To ensure that the membrane was in a consistent and pristine condition between different sets of comparative experiments, the following conventional cleaning protocol was applied to the ceramic nanofiltration membrane after each set of experiments:

1. Sodium hypochlorite (NaClO) cleaning: The membrane module was flushed in forward direction with a 0.2% NaClO solution for 30 min. NaClO is a strong oxidizing agent that effectively degrades and removes organic foulants (e.g., sodium alginate) adsorbed on the membrane surface and within the membrane pores [51].
2. Hydrochloric acid (HCl) cleaning: Subsequently, the membrane was rinsed with a 0.01 $mol{\cdot}L^{-1}$ HCl solution for 5 min to dissolve any inorganic precipitates (e.g., $CaCO_3$) that may have remained after the NaClO cleaning.
3. Demineralized water rinsing: Finally, the membrane was flushed with deionized water at a cross-flow velocity of 0.67 $m{\cdot}s^{-1}$ for 5 min to remove residual chemicals and restore membrane permeability.

After cleaning, the pure water permeability of the membrane was measured using deionized water at a constant flux of 20 $L{\cdot}m^{-2}{\cdot}h^{-1}$ and compared with the initial permeability to confirm that the membrane had been restored to a clean state (recovery rate $>$ 99%).

2.7. Three-dimensional excitation-emission matrix (3D-EEM) fluorescence spectroscopy

To characterize the fluorescence properties of organic matter in Schie Canal surface water, and specifically to assess the presence and relative abundance of humic-like components, three-dimensional excitation-emission matrix (EEM) spectra were acquired using a Hitachi F-7100 fluorescence spectrophotometer (Hitachi High-Tech Corporation, Tokyo, Japan) [52]. The excitation wavelength (Ex) was scanned from 200 to 400 nm at 10 nm intervals, and the emission wavelength (Em) was recorded from 280 to 550 nm at 5 nm intervals. Water samples were filtered through 0.45 μm polyethersulfone membrane filters immediately after collection. To eliminate the inner filter effect, each sample was diluted with Milli-Q water until the UV absorbance at 254 nm (UV_{254}) was below 0.05 cm^{-1} before EEM scanning [53].

2.8. X-ray diffraction (XRD) analysis

To identify the crystalline phases formed on the membrane surface, XRD analysis was performed on the $CaCO_3$ precoated membrane after treating Schie Canal water. The measurements were carried out using a Cu Kα radiation source ($\lambda = 1.5406$ Å) at a generator voltage of 40 kV and a current of 40 mA. The diffraction patterns were recorded over a 2θ range of 10° to 80° with a step size of 0.0302° [54]. The obtained patterns were compared with standard reference patterns from the International Centre for Diffraction Data database for phase identification.

2.9. Zeta potential measurement

To characterize the surface charge properties of the membranes under conditions relevant to the filtration experiments, zeta potential measurements were performed using a SurPASS electrokinetic analyzer (Anton Paar, Austria) with an adjustable gap cell. All measurements were conducted in a background electrolyte solution of 1 mM KCl at pH 7.5–8.0 (adjusted with HCl or NaOH as needed), matching the actual pH of Schie Canal water. The zeta potential was calculated from measured streaming potentials using the Helmholtz–Smoluchowski equation. For each membrane condition (pristine, $CaCO_3$-precoated, fouled, and citric acid-cleaned), three replicate measurements were performed, and the average values with standard deviations are reported.

3. Results and discussion

3.1. MWCO of the ceramic NF membrane

Fig. 3a presents the scanning electron microscopy (SEM) image of the internal structure of the pristine ceramic membrane, clearly showing the asymmetric multilayer architecture consisting of a porous α-Al_2O_3/γ-Al_2O_3 support layer and a thin TiO_2 separation layer. In Fig. S4, Energy-dispersive X-ray spectroscopy (EDS) analysis confirmed that the membrane was predominantly composed of Al_2O_3 (Table S2). MWCO analysis (Fig. 3b), conducted via polyethylene glycol (PEG) rejection experiments, demonstrated an experimental value of 591 *Da*, exceeding the manufacturer's value of 450 *Da*, yet remaining within the range of NF membranes [55,56]. This observation aligned with prior studies examining analogous membrane architectures [30,31].

3.2. Comparison analysis of model sewage with precoat and continuous dosing

The initial membrane permeability was determined to be 17 $L{\cdot}m^{-2}{\cdot}h^{-1}{\cdot}bar^{-1}$ through cross-flow filtration experiments using demineralized water as the feed solution. Considering the critical role of particle size in determining permeability recovery [29], a stable $CaCO_3$ suspension was prepared by adding 9 mM Ca^{2+} and 3 mM HCO_3^-. The resulting suspension exhibited a zeta potential of +24.8 mV and a uniform particle size of 0.187 μm (Fig. S1a) and remained well-dispersed without aggregation for 24 h. For the precoating experiments, the membrane surface was modified through dead-end filtration deposition of a $CaCO_3$ colloidal suspension (0.4 $g{\cdot}L^{-1}$ concentration) under a TMP of 9 bar and permeate flux of 110 $L{\cdot}m^{-2}{\cdot}h^{-1}$ for 7 min, to achieve a uniform coating distribution across the filtration surface. The precoats were produced with an identical mass of 1200 mg $CaCO_3$, which was equivalent to 11.5 $g{\cdot}m^{-2}$ membrane surface, while the continuous dosing process maintained a $CaCO_3$ dosage of 400 mg per operational cycle (1200 mg for the entire experiment). SEM images of the membrane surface after $CaCO_3$ deposition (Fig. S2a) revealed that, under the optimized deposition conditions (9 bar, 110 $L{\cdot}m^{-2}{\cdot}h^{-1}$, 7 min), $CaCO_3$ particles formed a relatively continuous and uniform coverage layer on the membrane surface. This morphological feature provides support for the subsequent "sacrificial protection" mechanism. Furthermore, MWCO analysis showed a slight decrease from 591 *Da* (pristine membrane) to approximately 577 *Da* after $CaCO_3$ deposition (Fig. S2b), indicating that the $CaCO_3$ particles did not completely block the membrane pores but rather formed an additional sacrificial layer on the membrane surface that can react with acid. The synthetic wastewater contained 3 mM $CaCl_2$ in addition to sodium alginate. The presence of Ca^{2+} ions is crucial because calcium ions interact with the carboxyl functional groups on alginate polymers, facilitating intermolecular crosslinking that forms the characteristic "egg-box" configuration [34]. Under these conditions, sodium alginate no longer exists as individual polymer chains but rather forms three-dimensional gel network structures. Dynamic light scattering measurements revealed that the average size of the synthesized sodium alginate aggregates was 33.04 μm (Fig. S1b).

Fig. S3 compares the membrane permeability recovery after citric acid cleaning for the sodium alginate fouling solution, with and without $CaCO_3$ precoating. The results show that without the precoating, citric acid cleaning was largely ineffective, achieving a recovery rate of only 14%. By contrast, with the $CaCO_3$ precoating, the recovery rate was improved (86%), indicating the role of the $CaCO_3$ precoating in citric acid cleaning. This is probably due to the chelating properties of citric acid [29]. The three carboxyl groups (–COOH) in its molecular structure exhibit a strong affinity for Ca^{2+} ions, and their reaction leads to the formation of complexes [57], which in turn promotes the structural loosening and detachment of the $CaCO_3$-sodium alginate composite layer. Meanwhile, the resulting high-molecular-weight chelates provide abundant adsorption sites for sodium alginate, enhancing its removal from the membrane surface during flushing, thereby achieving higher permeability recovery after citric acid cleaning [58]. Fig. 4a presents the permeability recovery for both the precoating and continuous coating methods after acid cleaning when treating synthetic wastewater. The precoating method showed better performance, achieving 95% recovery after the first acid-cleaning cycle and maintaining an 87% recovery after the second cycle (Table 1). The continuous dosing method showed lower recovery, attaining 82% and 59% after the first and second cleaning cycles, respectively. The IC analyses of Ca^{2+} ion concentration provided a quantitative determination of the $CaCO_3$ consumption during citric acid reactions. Fig. 4b revealed a higher $CaCO_3$ consumption during acid cleaning in the continuous dosing method (1933 $mg{\cdot}m^{-2}$ after the 1st cycle and 2335 $mg{\cdot}m^{-2}$ after the 2nd cycle, respectively) compared to the precoating method (1598 $mg{\cdot}m^{-2}$ after the 1st cycle and 1397 $mg{\cdot}m^{-2}$ after the 2nd cycle, respectively). In summary, the operational simplicity of the continuous dosing method came at the cost of higher $CaCO_3$ consumption and a suboptimal permeability recovery compared to the precoating method. To further evaluate the integrity of the $CaCO_3$ precoat layer and its ability to prevent foulant penetration, EDS analysis was performed on the membrane surface after precoating (Table S3). The results show that Ca and O together accounted for >95 at.% of the detected elements, while signals from the underlying membrane (Al and Ti) remained relatively low (Al: 0.67 at.%; Ti: 0.84 at.%), suggesting that the precoat layer was likely continuous rather than patchy. No fluorine (F) was detected, and other potential inorganic foulants such as

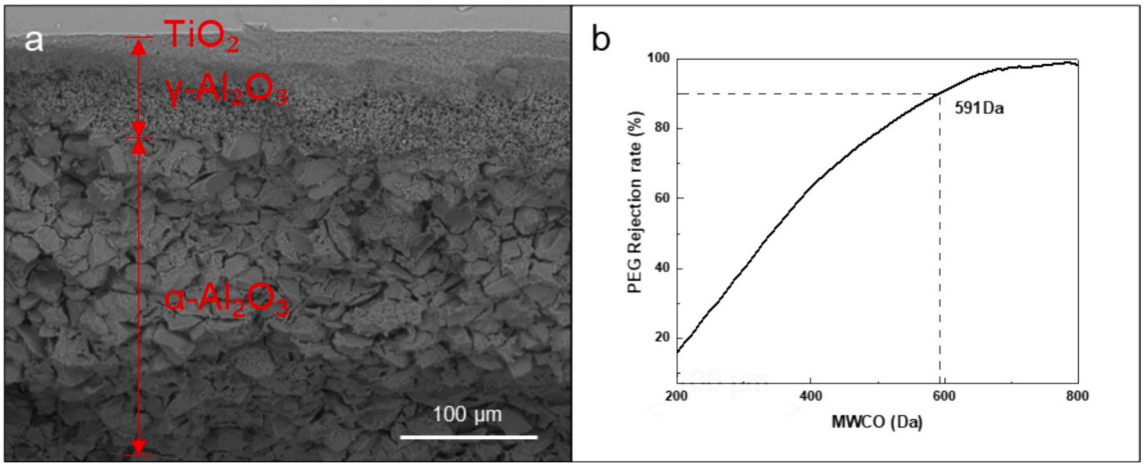


Fig. 3. (a) Cross-section of pristine membrane (b) determination of MWCO for the ceramic NF membranes through PEG rejection analysis.

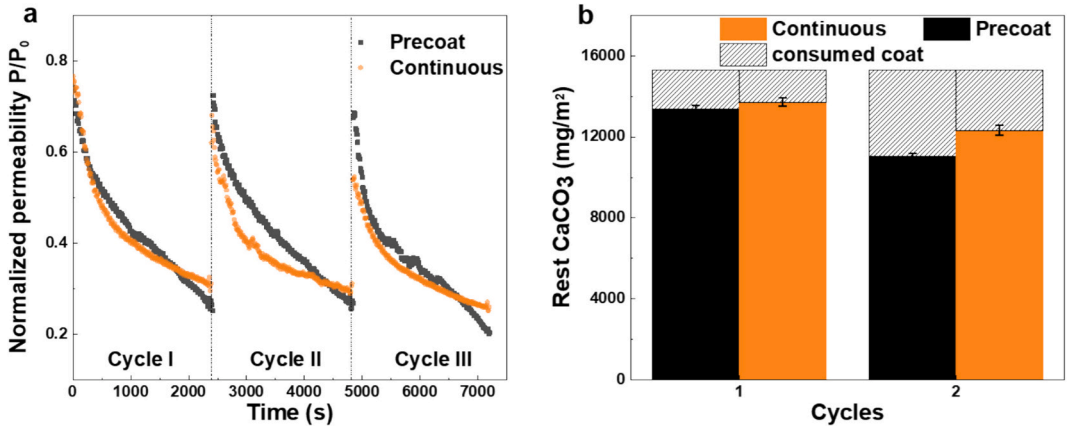


Fig. 4. (a) Normalized permeability changes with precoat and continuous dosing (b) comparison of continuous dosing and precoats consumption.

Table 1
Permeability recovery of model sewage with precoat and continuous dosing.

Citric acid cleaning	$CaCO_3$ premix	$CaCO_3$ precoat
First cleaning	82%	87%
Second cleaning	59%	82%

P, Mg, Si, and Cl were present only at trace levels (<0.3 at.%). These results suggest that the $CaCO_3$ precoat layer may have served as an effective physical barrier, largely preventing the penetration or deposition of feedwater constituents (particularly small anions like F^-) onto the active membrane surface during the precoating process.

3.3. *Restoration of permeability with and without coating with surface water*

For the experiment filtering surface water (Schie Canal), Fig. 5a illustrates the temporal evolution of membrane permeability for three ceramic membrane types, namely an uncoated membrane, a precoated membrane with $CaCO_3$, and a membrane that was subjected to continuous dosing of $CaCO_3$, during surface water treatment, evaluated through three consecutive 6-hour operational cycles. These results are consistent with the findings observed with synthetic wastewater that the precoated membrane demonstrated the best permeability recovery (Table 2), exhibiting the highest recovery, followed by the continuously dosed variant, which also considerably outperformed the uncoated ceramic NF membrane in fouling experiments. This is because, in the

Table 2
Permeability recovery of surface water with precoat and continuous dosing.

Citric acid cleaning	$CaCO_3$ premix	$CaCO_3$ precoat	Uncoated
First cleaning	80%	95%	39%
Second cleaning	51%	87%	2%

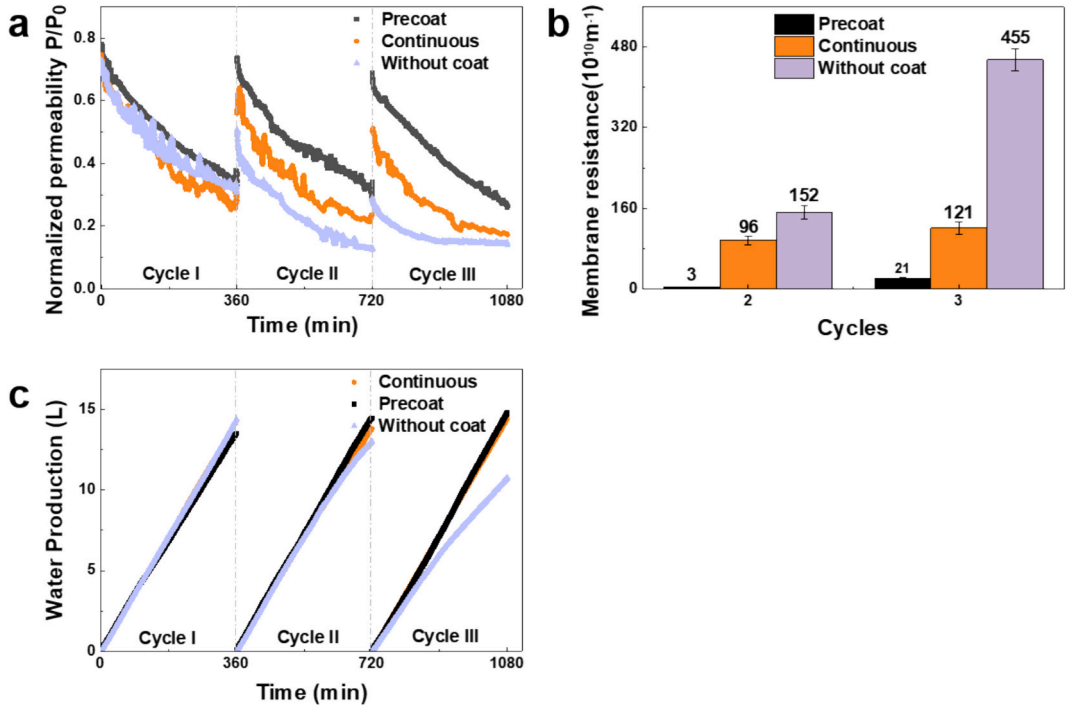


Fig. 5. (a) Normalized permeability changes with precoat, continuous dosing and without coat by treating surface water. (b) Irreversible membrane fouling resistance comparison of precoat, continuous dosing and without coating. (c) Comparison of water production performance of precoated, continuous dosing, and uncoated ceramic NF membranes during surface water filtration.

$CaCO_3$-foulant composite layer formed during surface water filtration, citric acid acts as a chelating agent [57], and its three carboxyl groups likewise exhibit a strong affinity for Ca^{2+} ions. By forming soluble calcium citrate complexes, citric acid effectively chelates the calcium ions within the $CaCO_3$ layer, thereby disrupting the "calcium bridge" structure between $CaCO_3$ particles and humic-like organic matter [59]. This calcium bridge structure is a key linkage between the carboxyl groups of humic substances and the $CaCO_3$ surface [60]. As the $CaCO_3$ layer dissolves and calcium ions are complexed and removed, the humic-mineral composite fouling layer originally attached to the membrane surface undergoes structural loosening and detachment [61]. Furthermore, the resulting high-molecular-weight chelates, such as calcium citrate, provide adsorption sites for dissolved humic substances, facilitating their removal from the membrane surface during flushing [29]. The enhanced recovery can be attributed to the $CaCO_3$ layer acting as a sacrificial barrier, a fouling mitigation strategy that has been shown to effectively shield the underlying membrane from direct contact with foulants [29]. In addition, the uncoated membrane showed higher permeability recovery when treating surface water (39% after the first cleaning, Table 2) compared to synthetic wastewater (14%). This discrepancy can be attributed to differences in foulant composition and cleaning mechanisms. For synthetic wastewater containing only sodium alginate, citric acid cleaning lacks specific chemical interactions with the polysaccharide gel layer, resulting in predominantly physical removal with limited efficacy. In contrast, surface water contains natural Ca^{2+} ions and humic-like substances. Even without a precoated layer, citric acid can chelate Ca^{2+} present in the fouling layer to form soluble calcium citrate complexes, thereby partially disrupting the calcium bridge structure between humic substances and mineral particles. This chemical interaction accounts for the moderately higher recovery observed for the uncoated membrane during surface water treatment. The recovery remained limited (39%) and decreased sharply to 2% after the second cycle, indicating progressive accumulation of irreversible fouling that citric acid alone cannot remove.

Fig. 5b presents a comparative analysis of irreversible fouling resistance among the three ceramic membrane types. It reveals that the precoated membrane exhibited the lowest irreversible fouling index (3×10^{10} m^{-1} vs 21×10^{10} m^{-1} after the 1st and 2nd cycles, respectively), suggesting its higher protective effect against contaminant adhesion and pore occlusion during surface water filtration, and thus a better permeability restoration compared to the membrane subjected to continuous dosing of $CaCO_3$. The lower irreversible fouling in precoated systems is consistent with the concept of forming a more porous and less compressible dynamic layer, which facilitated easier removal during chemical cleaning [62].

The consistent permeate output from the precoated and continuously dosed membranes, compared to the uncoated control, highlights the critical role of $CaCO_3$ coatings in maintaining a stable permeate production during a prolonged operation. Filtration performance monitoring (Fig. 5c) demonstrated that both the $CaCO_3$-precoated membrane and continuous dosing system maintained consistent permeate flux across operational cycles. The unmodified membranes exhibited a progressive flux decline, failing to sustain the target productivity of 40 $L{\cdot}m^{-2}{\cdot}h^{-1}$ under the system's maximum operating pressure of 10 bar. These findings established that the synergistic implementation of precoating and continuous dosing strategies with $CaCO_3$ and subsequent citric acid cleaning reduced fouling-induced efficacy losses and enhanced process robustness in demanding water purification applications.

The model wastewater experiments were conducted at a flux of 20 $L{\cdot}m^{-2}{\cdot}h^{-1}$ with 40 min filtration cycles to accelerate gel-layer fouling, whereas the surface water experiments were performed at 40 $L{\cdot}m^{-2}{\cdot}h^{-1}$ with 6 h cycles, which is more representative of practical operation. These differences in flux and filtration duration inevitably affect foulant deposition kinetics, cake layer structure, and compressibility, thereby influencing the observed permeability recovery.

Despite these limitations, the qualitative trend remains consistent: the $CaCO_3$ precoated membrane consistently outperformed the continuous dosing method, and both outperformed the uncoated membrane, regardless of the water matrix. The observed differences in recovery between the two water types can be attributed to several factors. First, foulant composition differs substantially: sodium alginate forms a relatively homogeneous polysaccharide gel, whereas Schie Canal water contains complex humic-like substances, particulates, and microorganisms that produce a more heterogeneous and mechanically stronger cake layer. Second, the ionic environment, particularly the higher Ca^{2+} concentration (3 mM) in the model wastewater versus around 1.2 mM in surface water, affects the extent of calcium bridging, which in turn influences the crosslinking density and acid-induced disruption efficiency of the fouling layer [63]. Third, the longer filtration duration in surface water experiments may allow for progressive consolidation and aging of the cake layer, making it more resistant to chemical cleaning [64].

The model wastewater experiments provide mechanistic insights under controlled conditions, whereas the surface water experiments are more representative of real-world performance. The consistent superiority of the precoating strategy across both systems supports its general applicability. Nevertheless, future studies employing identical flux and filtration duration for both water types, as well as testing a broader range of model foulants (e.g., protein-rich or algal organic matter), are recommended to enable more rigorous quantitative comparisons and to further delineate the applicability boundaries of this fouling control strategy.

3.4. Proposed cleaning mechanisms of coated and continuously dosed ceramic NF membranes

To investigate the interaction between $CaCO_3$ and humic-like substances, the 3D-EEM fluorescence spectra of Schie Canal water without $CaCO_3$ (Fig. 6a) and with $CaCO_3$ (Fig. 6b) were compared. As shown in Fig. 6a and b, both water samples exhibited multiple well-resolved fluorescence peaks in the region of Ex 200–400 nm and Em 280–550 nm, indicating the presence of various fluorescent organic components [65]. In Fig. 6a, two major humic-like fluorescence peaks were identified. The first was located at Ex 230–240 nm/Em 340–390 nm, with maximum intensities at Ex 240 nm/Em 365 nm (19.62 a.u.) and Ex 240 nm/Em 390 nm (16.96 a.u.), which is characteristic of UV humic-like substances. The second peak was observed at Ex 280–310 nm/Em 340–380 nm, with the strongest signal at Ex 280 nm/Em 340 nm (33.93 a.u.), corresponding to visible humic-like substances. After the addition of $CaCO_3$, a decrease in fluorescence intensity was observed for most humic-like peaks (Fig. 6b). This effect likely results from complexation between Ca^{2+} ions on the $CaCO_3$ surface and the carboxyl and phenolic groups of humic-like molecules. Such interactions alter molecular structure and reduce fluorescence quantum yield. [61]. However, not all peaks showed quenching. The peak at Ex 250 nm / Em 390 nm increased from 16.96 to 22.56 a.u. after $CaCO_3$ addition, suggesting that the adsorption of humic-like substances onto $CaCO_3$ particles may locally concentrate the fluorophores and partially enhance the fluorescence signal [66]. Meanwhile, the peak at Ex 240 nm/Em 360 nm remained relatively stable (from 19.62 to 18.76 a.u.), indicating that different fluorophores exhibit varying sensitivities to Ca^{2+} complexation. These results demonstrate that $CaCO_3$ alters the fluorescence properties of humic-like substances through combined complexation and adsorption effects.

The antifouling performance of the precoated membrane was demonstrated by its higher permeability recovery and lower irreversible fouling during surface water filtration (Fig. 5a, b; Table 2). To further confirm that this improved fouling resistance was not achieved at the expense of water quality, EEM analysis was performed on the permeate samples. For the precoated membrane (Fig. 6d), the fluorescence intensities of humic-like peaks were reduced to a similar extent for the uncoated membrane (Fig. 6c), with removal rates of approximately 91%

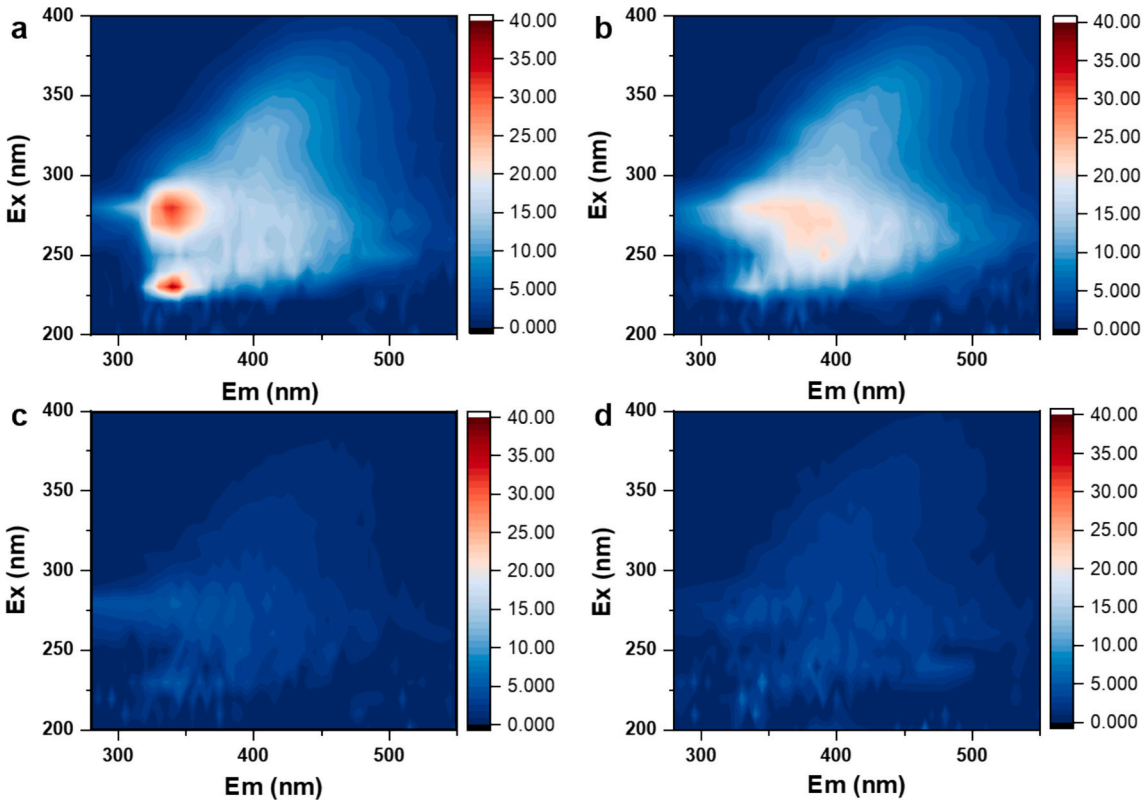


Fig. 6. Comparison of 3D-EEM fluorescence spectra of Schie Canal water: (a) without $CaCO_3$, (b) with $CaCO_3$ addition, (c) without $CaCO_3$ after filtration (d) with $CaCO_3$ addition after filtration.

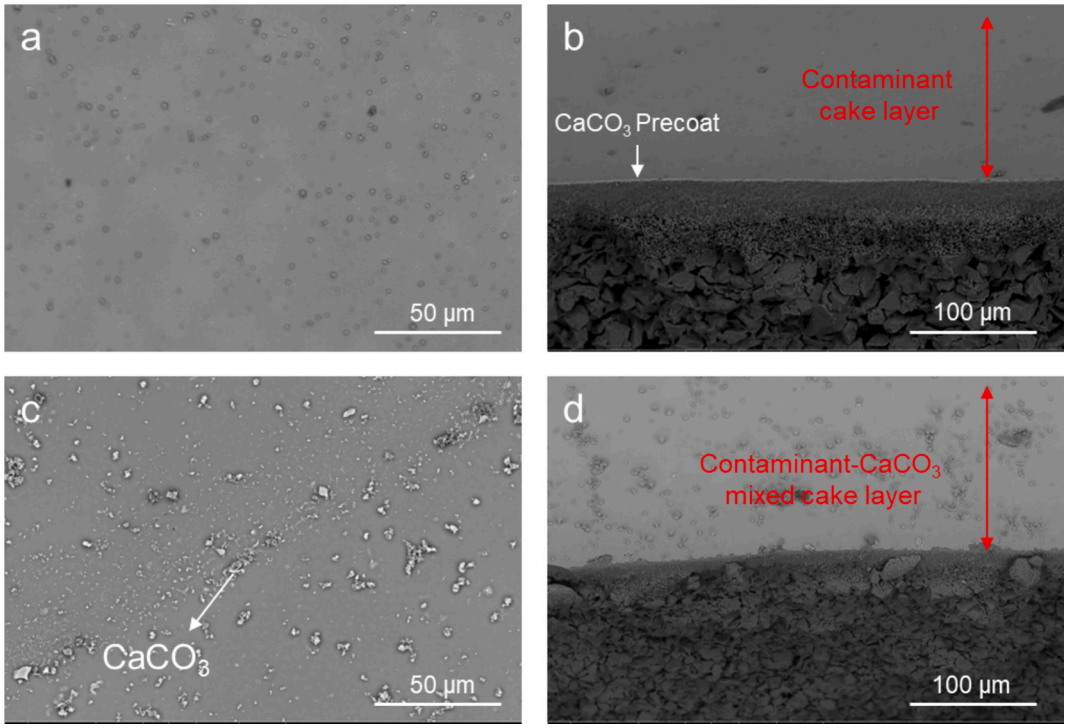


Fig. 7. SEM images of (a) Top-section view of $CaCO_3$ precoating with a contaminant cake layer on the membrane surface; (b) cross-section view of $CaCO_3$ precoating with a contaminant cake layer; (c) top-section view of $CaCO_3$ premixed with a contaminant cake layer on the membrane surface; (d) cross-section view of $CaCO_3$ premixed with a contaminant cake layer.

and 90%, respectively. This indicates that the $CaCO_3$ precoat layer, while serving as a sacrificial barrier to mitigate fouling [67], does not compromise the membrane's intrinsic separation capability for humic-like organic matter.

Moreover, the surface water used in this study (Schie Canal water) was characterized by a predominance of humic-like substances, as confirmed by 3D-EEM analysis, while sodium alginate served as a model polysaccharide foulant rich in carboxyl groups. The proposed $CaCO_3$ precoating/citric acid cleaning strategy relies on the formation of calcium bridges between Ca^{2+} ions and the carboxyl groups of organic foulants. Thus, this strategy is expected to be highly effective in waters containing sufficient Ca^{2+} (at least mM level) and carboxyl-rich organic matter, such as municipal wastewater and many surface waters. For waters with high protein content, which also contain carboxyl groups (e.g., from glutamic and aspartic acids), the strategy may remain effective. However, for waters dominated by algal organic matter, characterized by neutral polysaccharides and hydrophobic components with low carboxyl density, the calcium bridging effect may be weaker, potentially reducing cleaning efficiency. The applicability boundary of this strategy is therefore suggested for waters where carboxyl-rich organic matter and sufficient Ca^{2+} coexist. Future studies using waters with different organic compositions (e.g., protein-rich or algal organic matter-dominated waters) are needed to validate this strategy.

Fig. 7 presents a comparative analysis of two distinct interaction modes between $CaCO_3$ and the surface water contaminant layer on the membrane surface. In the precoating configuration (Fig. 7a and b), fine and uniformly distributed $CaCO_3$ particles were observed to cover the membrane surface, forming a continuous mineralized pre-layer, as shown in the top-view image (Fig. 7a). The corresponding cross-sectional view (Fig. 7b) confirmed a stratified structure: a dense $CaCO_3$ precoating was directly adhered to the membrane surface, overlaid by a contaminant layer. In comparison, under the premixed-condition scenario (Fig. 7c and d), $CaCO_3$ crystals appeared embedded within the contaminant matrix rather than forming a distinct underlying stratum. The surface view (Fig. 7c) revealed larger, irregularly shaped $CaCO_3$ aggregates dispersed throughout the contaminant material. The cross-sectional image (Fig. 7d) further illustrated a heterogeneous composite scale, wherein inorganic $CaCO_3$ particles and organic/colloidal foulants were interwoven uniformly across the layer thickness, with no discernible interface between the inorganic scale and the organic deposit. The elemental composition and distribution of the formed layers were characterized through EDS. Fig. S5 and its corresponding quantitative data in Table S4 present the EDS mapping and elemental analysis of the $CaCO_3$ precoating overlaid with a contaminant cake layer on the membrane surface (Corresponding to Fig. 7a). Similarly, Fig. S6 and Table S5 provided the EDS images and quantitative results for the composite layer formed when $CaCO_3$ was premixed within the contaminant cake (Corresponding to Fig. 7b). These results demonstrated that the $CaCO_3$ precoating method led to a clearly stratified fouling architecture, whereas the in-situ formation of $CaCO_3$ in the presence of contaminants produced a more intricate and monolithic organic–inorganic composite scale layer.

The comparative morphological analysis of acid reaction behaviors between the precoated and continuously dosed membranes was presented in Fig. 8, following fouling experiments using Schie Canal water. A digital microscope was first employed to examine the initial surface morphology of the pristine membrane (Fig. 8a). Characterization via digital microscopy distinctly revealed that the precoating method produced a uniform and continuous $CaCO_3$ deposition layer on the membrane surface (Fig. 8b). The continuous dosing process resulted in $CaCO_3$ crystals being embedded and dispersed within the organic cake layer formed by foulants from the surface water (Fig. 8d). Upon citric acid treatment, both configurations exhibited active bubble generation due to the chemical reaction between $CaCO_3$ and acid (Fig. 8c and Fig. 8e). However, the precoated membrane showed visibly fewer bubbles compared to the continuously dosed system. This observed difference in CO_2 release was directly correlated with the previously quantified higher $CaCO_3$ consumption in the continuous dosing method, thereby confirming a clear divergence in reaction intensity and efficiency between the two fouling control strategies.

This phenomenon probably involves two distinct mechanisms. The continuous dosing method resulted in an expanded interfacial contact area, which facilitated the thorough premixing of $CaCO_3$ particles with the contaminated solution, thereby enhancing reaction efficiency [68]. The observation that the precoating method achieved better cleaning efficacy than continuous dosing, despite lower total $CaCO_3$ consumption and less bubble generation, likely arises from the different spatial distribution of reaction sites. In the precoating configuration, $CaCO_3$ forms a layer directly on the membrane surface beneath the foulant cake (Fig. 9a). When citric acid reaches this layer, CO_2 bubbles are generated

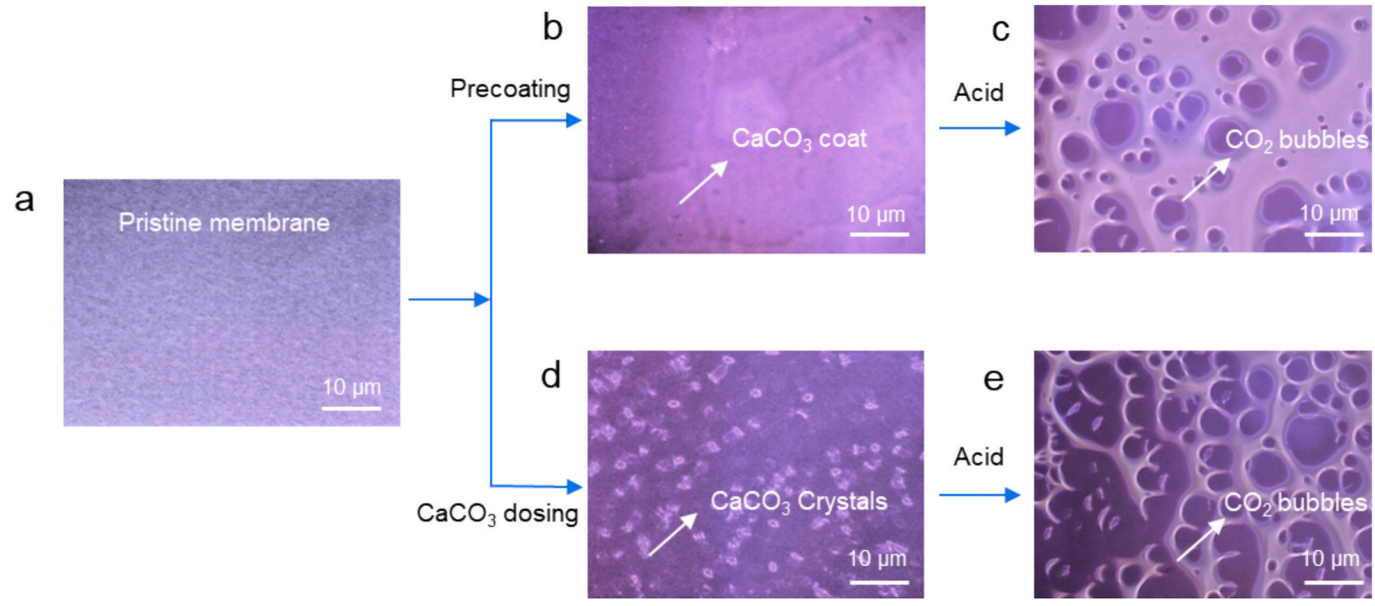


Fig. 8. Comparative analysis of membrane surface modifications under digital microscopes: (a) Pristine membrane (b) $CaCO_3$ precoat (c) precoat with citric acid reaction (d) continuous dosing with $CaCO_3$ (e) continuous dosing with citric acid reaction.

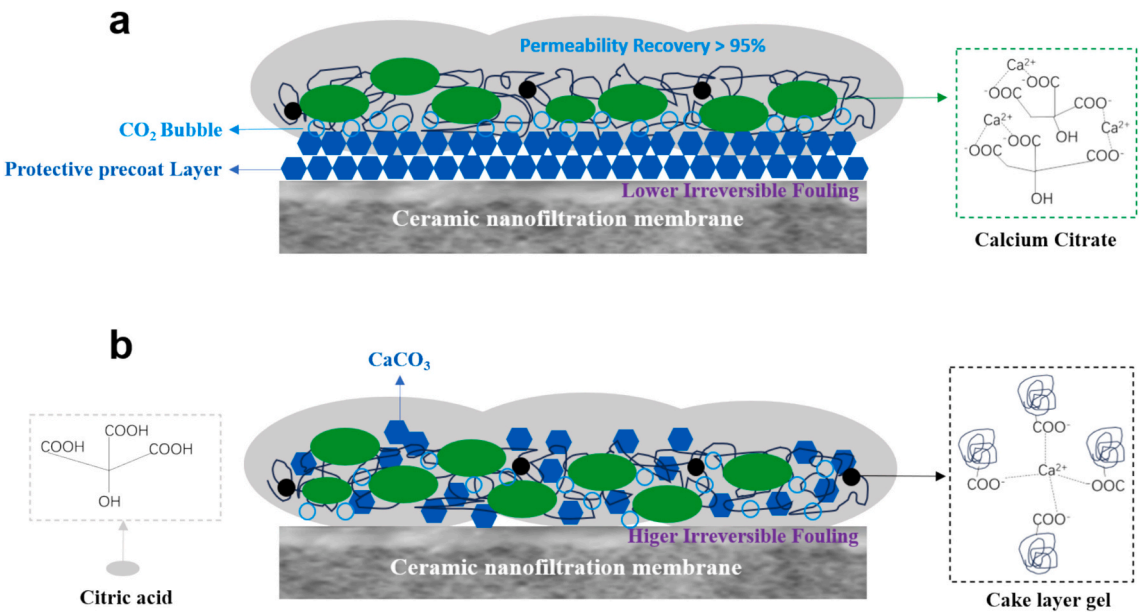


Fig. 9. Mechanistic demonstration of precoating [29] and continuous dosing techniques with $CaCO_3$ combined with citric acid cleaning for ceramic NF membranes.

at or near the membrane–foulant interface. This could help loosen the foulant layer from underneath [69]. By contrast, in the continuous dosing configuration, $CaCO_3$ particles are dispersed throughout the cake layer (Fig. 9b), and CO_2 bubbles form at various positions within the cake rather than preferentially at the membrane surface [70]. This difference in bubble location may contribute to the observed difference in cleaning efficiency. Direct visualization and quantitative mechanical analysis are needed to fully validate this mechanism.

3.5. Rejection performance of coated and continuously dosed ceramic membranes

The removal performance of the precoated, continuous dosing, and uncoated ceramic NF membranes during the treatment of Schie Canal surface water is comprehensively summarized in Table 4 and Fig. 10. Although the uncoated membrane achieved a relatively high DOC removal rate (90%), its rejection of divalent cations (Ca^{2+}: 51%, Mg^{2+}: 61%) and specific anions (F^-: 44%, PO_4^{3-}: 55%) was limited. The

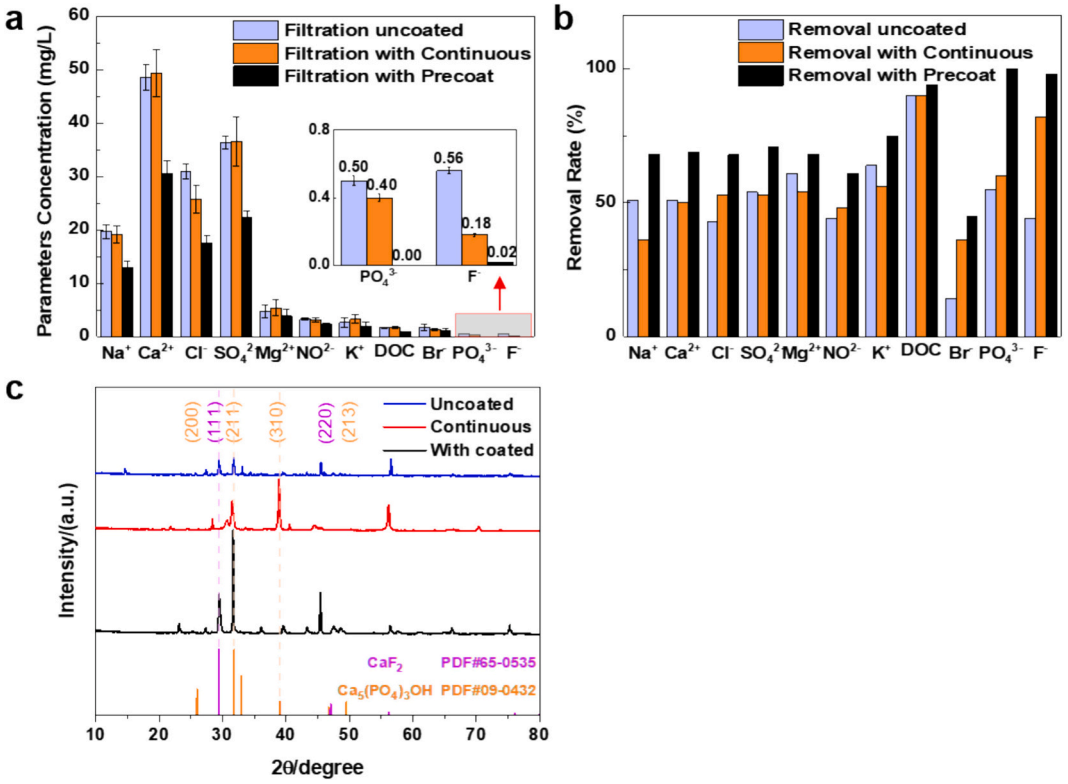


Fig. 10. (a) Water quality parameter test with coating and continuous dosing treatment. (b) Parameter removal after filtration with coating and continuous dosing treatment. (c) XRD patterns of continuous dosing and $CaCO_3$ precoated membrane surface after treating Schie Canal water.

continuously dosed membrane showed slightly improved performance compared to the uncoated membrane, with comparable DOC removal (90%) and marginally enhanced conductivity reduction (43%). The continuously dosed membrane showed improved rejection of F^- (82%) and PO_4^{3-} (60%), suggesting that the presence of $CaCO_3$ within the fouling layer contributed to enhanced retention of specific anions through chemical interactions. The precoated membrane exhibited the highest overall rejection performance across all measured parameters (Fig. 10). Zeta potential measurements (Table 3) show that the pristine membrane is negatively charged (−15.0 ± 3.75 mV), while the $CaCO_3$ precoat reverses the surface charge to weakly positive (+10.1 ± 3.39 mV). This charge reversal promotes electrostatic repulsion of divalent cations (Ca^{2+} and Mg^{2+} > 68%), alongside other mechanisms including dynamic filtration and cake-enhanced concentration polarization. This charge reversal indicates that the $CaCO_3$ layer imparts a weak positive charge to the membrane surface, thereby enabling electrostatic repulsion of divalent cations (Ca^{2+}, Mg^{2+}). The precoated membrane thus achieved higher rejections of divalent cations (>68%) compared to the pristine membrane (51–61%). Following fouling with Schie Canal water, the zeta potential decreased to +5.87 ± 0.4 mV, likely due to partial neutralization by negatively charged NOM adsorbed on the surface. Still, the surface remained weakly positive, suggesting that electrostatic repulsion of cations may still be partially effective during filtration. After citric acid cleaning, the zeta potential became nearly neutral at +2.84 ± 0.2 mV, indicating effective removal of the $CaCO_3$ precoat and most foulants, consistent with the high permeability recovery (95%). The incomplete return to the pristine negative value may be due to trace citrate adsorption or minor surface alterations, but this did not compromise subsequent recoating or overall membrane performance. The synergistic interaction between the positively charged precoat and the negatively charged membrane surface selectively improved the rejection of divalent cations [71]. This modification enhanced both electrostatic repulsion against similarly charged ions and steric hindrance, thereby improving the selective retention of divalent species [72]. The exceptional removal efficiencies for specific anions, F^- and PO_4^{3-}, exceeded 98%. These high rejection values were likely driven by specific chemical interactions rather than purely physical mechanisms. These high rejection values could be attributed to the potential in situ formation of poorly soluble compounds, such as fluorite (CaF_2) or hydroxyapatite ($Ca_5(PO_4)_3OH$), within or atop the filtration layer. This phenomenon aligns with previously reported mechanisms of precipitation-enhanced filtration, where dissolved ions react to form insoluble precipitates that are subsequently retained [73]. In addition to this charge effect, the porous $CaCO_3$ layer acts as a dynamic filtration barrier, while cake-enhanced concentration polarization and adsorption/complexation with the precoat and organic matter may also contribute to cation retention. Unlike the bare membrane, where Donnan exclusion is the primary mechanism [74], the precoated system combines dynamic-layer filtration with chemical interactions. XRD analysis of the precoated membrane surface revealed diffraction peaks at 2θ ≈ 29.3° corresponding to CaF_2, as well as peaks at 2θ ≈ 31.8° (PDF #09-0432) corresponding to $Ca_5(PO_4)_3OH$ (Fig. 10c). In contrast, the uncoated membrane showed no detectable crystalline phases of these sparingly soluble salts under identical measurement conditions, consistent with the low solid mass expected on the bare membrane surface. The continuously dosed membrane exhibited clear $CaCO_3$ peaks but only weak, near-background signals for $Ca_5(PO_4)_3OH$ and no detectable CaF_2. These comparative data are consistent with the occurrence of precipitation-enhanced rejection on the precoated membrane, where the sacrificial $CaCO_3$ layer may serve as a reactive substrate for the in-situ formation of CaF_2 and $Ca_5(PO_4)_3OH$. However, the relatively weak intensity of these precipitate peaks (compared to the dominant $CaCO_3$ pattern) suggests that precipitation is not the sole rejection mechanism; size exclusion and charge effects also contribute to the observed high removals (F^- and PO_4^{3-} > 98%). The precipitation mechanism is therefore proposed as an additional and enhanced factor rather than the exclusive pathway for anion rejection. The EDS analysis of the precoated membrane surface after filtration (Table S3) reveals the coexistence of Ca, F, and P on the membrane surface, with Ca being the dominant element (26.93 at.%) and F and P present at 0.001 at.% and 0.17 at.%, respectively. Although these are not elemental distribution maps, the simultaneous presence of these elements on the membrane surface is consistent with the in-situ formation of sparingly soluble CaF_2 and calcium phosphate species within the $CaCO_3$ precoat layer. This elemental co-localization, together with the XRD peaks corresponding to CaF_2 and $Ca_5(PO_4)_3OH$ (Fig. 10c), supports the interpretation that the high removals of F^- and PO_4^{3-} (>98%) may be at least partially attributed to precipitation-enhanced rejection. The CaF_2 diffraction peak at 2θ ≈ 29.3° (PDF #65-0535) partially overlaps with the main calcite ($CaCO_3$) peak at 2θ ≈ 29.4° (PDF #05-0586), which limits the precision of CaF_2 identification solely by XRD. Nevertheless, the $Ca_5(PO_4)_3OH$ peaks at 2θ ≈ 25.9° and 33.0° are more distinct and less affected by $CaCO_3$ overlap, providing clearer evidence for phosphate precipitation. In addition, the significant difference in fluoride rejection between the precoated (98%) and continuously dosed (82%) membranes, combined with the EDS data showing F on the precoated membrane surface (Table S3) and the XRD control patterns (Fig. S7), collectively supports the occurrence of precipitation-enhanced rejection.

The continuously dosed membrane also showed enhanced F^- and PO_4^{3-} rejection (82% and 60%, respectively) compared to the uncoated membrane, further supporting the role of $CaCO_3$ in facilitating these chemical interactions. The high rejection rates of fluoride and phosphate (>98%) observed with the $CaCO_3$ precoated membrane do not imply conventional mineral scaling on the active NF membrane surface. Rather, the precipitation of sparingly soluble compounds such as CaF_2 or $Ca_5(PO_4)_3OH$ occurs within the sacrificial $CaCO_3$ precoat layer, rather than directly on the underlying TiO_2 separation layer. Since both $CaCO_3$ and any co-precipitated CaF_2 or calcium phosphate are soluble under acidic conditions (citric acid, pH 2.9), the same cleaning step that removes the precoat layer also removes any inorganic precipitates that have formed. This is fundamentally different from scaling on the surface of a conventional bare membrane, which is typically irreversible and resistant to mild acid cleaning [75].

Furthermore, the treatment process achieved a substantial reduction

Table 3
Zeta potential of the ceramic NF membrane surface under different conditions.

Membrane condition	Zeta potential (mV)
Pristine (uncoated)	−15.0 ± 3.75
$CaCO_3$-precoated	+10.1 ± 3.39
Fouled (after surface water filtration)	+5.87 ± 0.4
Citric acid-cleaning	+2.84 ± 0.2

Table 4
Water quality parameters of Schie Canal water before and after filtration.

	Units	Schie Canal water	Filtration without coat	Filtration with continuous	Filtration with coat
pH	–	8.1	8.0	8.0	8.0
Conductivity	μS/cm	747	440	427	245
DOC	mg/L	16.7	1.7	1.8	0.9
Na^+	mg/L	40.5	19.7	19.2	13.0
K^+	mg/L	7.5	2.7	3.3	1.9
Mg^{2+}	mg/L	11.9	4.7	5.4	3.9
Ca^{2+}	mg/L	98.4	48.6	49.3	30.6
F^-	mg/L	1.0	0.56	0.18	0.02
Cl^-	mg/L	54.3	30.9	25.7	17.6
Br^-	mg/L	2.1	1.8	1.4	1.2
NO_2^-	mg/L	5.9	3.3	3.1	2.3
PO_4^{3-}	mg/L	1.1	0.5	0.4	0.0
SO_4^{2-}	mg/L	78.1	36.3	36.6	22.4

in bulk water parameters, a 65% decrease in electrical conductivity and a 94% removal of DOC. These results underscore the system's dual capability for effective desalination and concurrent removal of organic contaminants. The high DOC removal was presumably the result of a synergistic effect: the refined membrane pore structure provided enhanced size-based exclusion, while the accumulated cake layer itself exhibited a high affinity for adsorbing and retaining organic molecules. This combined mechanism has been documented in other studies involving layered or dynamically formed membrane systems [18]. Our findings highlight the superior multifunctional performance of the $CaCO_3$ precoating strategy compared to both the continuous dosing approach and uncoated membranes. While the uncoated membrane demonstrated baseline rejection capabilities and the continuously dosed membrane showed moderate improvements (particularly for F^- and PO_4^{3-}), the precoating method demonstrated not only effective fouling control but also robust, simultaneous removal of a wide spectrum of contaminants, including ions, salts, and organic matter. This positions it as a promising strategy for advanced water treatment applications that demand high-efficiency, multi-contaminant removal capabilities. The high permeability recoveries (Table 2) observed after citric acid cleaning suggest that no irreversible scaling occurred on the active membrane layer. To further assess the reversibility of the precipitation-enhanced rejection, EDS analysis was performed on the membrane surface after the final cleaning protocol (NaClO + HCl). As shown in Table S6, only trace amounts of Mg^{2+} were detected on the membrane surface, while no clear Ca, F, or P signals were observed. The pure water permeability recovered to >99% of its initial value after this cleaning procedure. These results suggest that both the sacrificial $CaCO_3$ layer and any co-precipitated CaF_2 or $Ca_5(PO_4)_3OH$ were completely removed, leaving the active TiO_2 layer substantially free of inorganic residues. The minor Mg^{2+} is likely attributed to the weaker complexation affinity of citric acid for Mg^{2+} compared to Ca^{2+}, and its presence does not compromise membrane performance. XRD analysis of the membrane surface after citric acid cleaning was attempted but could not be reliably performed due to the very low solid mass remaining on the membrane surface. This is consistent with the high permeability recovery (>95%) and the EDS results (Table S6), which show no detectable Ca, F, or P signals after cleaning, suggesting that both the sacrificial $CaCO_3$ layer and any co-precipitated CaF_2 or $Ca_5(PO_4)_3OH$ were effectively removed.

3.6. Preliminary environmental and economic considerations

The use of chemical cleaning agents in membrane fouling control inevitably raises concerns about chemical emissions and resource consumption [76]. In this study, citric acid was employed as the primary cleaning agent, rather than mineral acids such as HCl or oxidizing agents like NaClO. Citric acid is a biodegradable organic acid [77], and compared to mineral acids produced through energy-intensive industrial processes (e.g., the chlor-alkali process for HCl), it may offer certain environmental advantages. A low concentration of HCl (0.01 $mol \cdot L^{-1}$) was used only as a supplementary 5-minute rinse in the final rigorous cleaning protocol to dissolve residual $CaCO_3$ deposits after NaClO treatment, and this step is not part of the routine fouling control cycles.

The following discussion is a preliminary, qualitative consideration rather than a full environmental or economic assessment. Several important factors, including energy consumption for precoating deposition, pumping and mixing requirements, chemical transport, waste-liquid handling, sludge or precipitate disposal, membrane lifespan, cleaning frequency, operational downtime, and labor costs, are not yet accounted for in this analysis.

The proposed strategy has several potentially favorable features that require further investigation. The precoated membrane retained 87% of its permeability after the second cycle (Table 2), while the uncoated membrane recovered only 2%. Because the uncoated membrane does not benefit from the $CaCO_3$/citric acid reaction mechanism, it would require more frequent chemical cleaning to sustain operation in practice. Over the same three operational cycles, both the precoating and continuous dosing methods consumed only one-third of the NaClO used by a conventional cleaning approach that requires chemical cleaning in every cycle. By mitigating irreversible fouling, this strategy could potentially extend the effective lifespan of the ceramic membrane [76], although long-term validation is needed. In addition, conventional fouling control often relies on NaClO, whose production via chlor-alkali electrolysis is energy-intensive and can generate toxic byproducts such as adsorbable organic halides [78]. Conversely, citric acid is produced via fermentation.

In terms of economic feasibility, based on market price data as of January 2026 compiled from ChemicalBook ($CaCO_3$: approximately €60 per ton; citric acid: approximately €550 per ton; 10% NaClO: approximately €68 per ton; exchange rate: €1 ≈ $1.17, as of January 2026), the material cost per cycle for the $CaCO_3$ precoating/citric acid cleaning strategy is estimated to be approximately €0.01 (consuming 1.2 g of $CaCO_3$ and the corresponding amount of citric acid), whereas conventional chemical cleaning (NaClO) costs approximately €0.043 per cycle at lab scale. However, this estimate covers only direct material costs and does not include energy consumption for dosing, water loss during cleaning, sludge handling and disposal, membrane replacement frequency, or labor costs. Therefore, this cost comparison should be viewed as a rough indication of material expenses only, and not as a comprehensive economic evaluation.

Regarding energy consumption associated with pumping operations, the precoating deposition step requires pumping the $CaCO_3$ suspension through the membrane module for approximately 7 min per cycle at 8–10 bar, whereas continuous dosing requires only premixing of $CaCO_3$ with the feed water (negligible additional energy). Based on the membrane area (0.1045 m^2) and flux (110 $L \cdot m^{-2} \cdot h^{-1}$) used in this study, the estimated pumping energy for precoating deposition is approximately 0.02–0.03 kWh per cycle. This estimate is provided as a preliminary indication and does not represent a complete energy balance, as it does not account for energy associated with chemical production, transport, or waste treatment. When normalized to the volume of water treated per cycle (approximately 1.4 L), the absolute energy difference between the two strategies is small. Furthermore, the continuous dosing strategy consumes substantially more $CaCO_3$ and achieves lower permeability recovery, which may lead to more frequent cleaning and higher overall energy demand in the long term. In summary, while the $CaCO_3$ precoating/citric acid cleaning strategy shows several potentially favorable features from environmental and economic angles, a full life-cycle assessment, chemical discharge analysis, sludge handling evaluation, and long-term operational cost analysis are needed before drawing solid conclusions about its overall sustainability and cost-effectiveness.

4. Conclusion and perspective

This study presents a comparative analysis of $CaCO_3$ precoating of ceramic NF membranes versus continuous dosing of $CaCO_3$ to ceramic NF membranes. The conclusions are summarized as follows:

- A comparative analysis of the experimental results revealed that while the continuous dosing method also exhibited good permeability recovery, the precoated membranes exhibited superior performance in both synthetic and real water matrices.
- The $CaCO_3$ precoat was successfully and uniformly applied to the membranes using a dead-end filtration process. When treating natural surface water, these precoated membranes achieved the highest levels of permeability restoration and, critically, the lowest degree of irreversible fouling. This was quantitatively demonstrated by its lower irreversible fouling resistance after the second operational cycle (3×10^{10} m^{-1}), compared to the continuous dosing (21×10^{10} m^{-1}) and uncoated membrane (72×10^{10} m^{-1}). The proposed mechanism for this improvement was attributed to the precoat layer acting as a protective barrier. It likely reduced direct foulant

adhesion by acting as a protective sacrificial barrier, thereby mitigating irreversible fouling.

- Water quality data from the feed and permeate of the ceramic NF membrane systems treating Schie Canal water demonstrate that the precoated membranes performed well in electrical conductivity reduction (65%) and DOC removal (94%). Divalent ions (Ca^{2+}, Mg^{2+} > 68%) and anions (F^-, PO_4^{3-} > 98%) also exhibited high rejection efficacies.
- Preliminary environmental and economic considerations indicate that the $CaCO_3$ precoating/citric acid cleaning strategy uses a biodegradable organic acid and shows lower direct material costs compared to conventional NaClO-based cleaning at lab scale. However, the precoating deposition step requires additional pumping energy, and a full life-cycle assessment is needed before definitive conclusions can be drawn regarding its overall sustainability and cost-effectiveness.
- Future work using interrupted cleaning experiments, in situ visualization with transparent model systems, and COMSOL simulations of bubble nucleation, growth, and interfacial shear stress are needed to quantitatively validate the proposed bubble-mediated detachment mechanism.
- This study focuses on short-term antifouling performance. Long-term stability and durability under realistic conditions have not been systematically evaluated. Key aspects, such as flux decline, fouling development, permeability recovery after repeated cleaning, residual $CaCO_3$ accumulation, and temporal changes in ion rejection, require further investigation through extended filtration experiments (e.g., around 15 days of continuous or cyclic operation). The current findings represent lab-scale proof-of-concept evidence and are not sufficient to support full-scale implementation. Future work will include pilot-scale and long-term operational studies to validate this strategy under practical conditions.

CRediT authorship contribution statement

Yuke Li: Conceptualization, Methodology, Investigation, Data curation, Writing – original draft, Writing – review & editing. **Luuk C. Rietveld:** Writing – review & editing, Funding acquisition, Supervision. **Sebastiaan G.J. Heijman:** Conceptualization, Methodology, Funding acquisition, Writing – review & editing, Supervision.

Declaration of competing interest

The authors declare that they have no known competing financial interests or personal relationships that could have appeared to influence the work reported in this paper.

Acknowledgement

The authors acknowledge the PhD scholarship awarded to Yuke Li (No. 201907720010) by the China Scholarship Council, China.

Appendix A. Supplementary data

Supplementary data to this article can be found online at https://doi.org/10.1016/j.desal.2026.120502.

Data availability

Data will be made available on request.

References

[1] P. Goh, A. Ismail, A review on inorganic membranes for desalination and wastewater treatment, Desalination 434 (2018) 60–80, https://doi.org/10.1016/j.desal.2017.07.023.
[2] X. Zheng, Z. Zhang, D. Yu, X. Chen, R. Cheng, S. Min, J. Wang, Q. Xiao, J. Wang, Overview of membrane technology applications for industrial wastewater treatment in China to increase water supply, Resour. Conserv. Recycl. 105 (2015) 1–10, https://doi.org/10.1016/j.resconrec.2015.09.012.
[3] J. Gurauskis, Ø.F. Lohne, H.L. Lein, K. Wiik, Processing of thin film ceramic membranes for oxygen separation, J. Eur. Ceram. Soc. 32 (3) (2012) 649–655, https://doi.org/10.1016/j.jeurceramsoc.2011.10.009.
[4] Q. Zhang, Y. Fan, N. Xu, Effect of the surface properties on filtration performance of Al2O3–TiO2 composite membrane, Sep. Purif. Technol. 66 (2) (2009) 306–312, https://doi.org/10.1016/j.seppur.2008.12.010.
[5] M.B. Asif, Z. Zhang, Ceramic membrane technology for water and wastewater treatment: a critical review of performance, full-scale applications, membrane fouling and prospects, Chem. Eng. J. 418 (2021) 129481, https://doi.org/10.1016/j.cej.2021.129481.
[6] R. Jarrar, M. Abbas, M. Al-Ejji, Environmental remediation and the efficacy of ceramic membranes in wastewater treatment—a review, Emerg. Mater. 7 (4) (2024) 1295–1327, https://doi.org/10.1007/s42247-024-00687-0.
[7] M. Chen, S.G. Heijman, L.C. Rietveld, Ceramic membrane filtration for oily wastewater treatment: basics, membrane fouling and fouling control, Desalination (2024) 117727, https://doi.org/10.1016/j.desal.2024.117727.
[8] M. Chen, S.G. Heijman, L.C. Rietveld, State-of-the-art ceramic membranes for oily wastewater treatment: modification and application, Membranes 11 (11) (2021) 888, https://doi.org/10.3390/membranes11110888.
[9] H. Xu, K. Xiao, X. Wang, S. Liang, C. Wei, X. Wen, X. Huang, Outlining the roles of membrane-foulant and foulant-foulant interactions in organic fouling during microfiltration and ultrafiltration: a mini-review, Front. Chem. 8 (2020) 417, https://doi.org/10.3389/fchem.2020.00417.
[10] L.Y. Ng, A.W. Mohammad, C.P. Leo, N. Hilal, Polymeric membranes incorporated with metal/metal oxide nanoparticles: a comprehensive review, Desalination 308 (2013) 15–33, https://doi.org/10.1016/j.desal.2010.11.033.
[11] D. Rana, T. Matsuura, Surface modifications for antifouling membranes, Chem. Rev. 110 (4) (2010) 2448–2471, https://doi.org/10.1021/cr800208y.
[12] R.R. Choudhury, J.M. Gohil, S. Mohanty, S.K. Nayak, Antifouling, fouling release and antimicrobial materials for surface modification of reverse osmosis and nanofiltration membranes, J. Mater. Chem. A 6 (2) (2018) 313–333, https://doi.org/10.1039/C7TA08627J.
[13] B. Díez, R. Rosal, A critical review of membrane modification techniques for fouling and biofouling control in pressure-driven membrane processes, Nanotechnol. Environ. Eng. 5 (2) (2020) 15, https://doi.org/10.1007/s41204-020-00077-x.
[14] C. Panchal, J. Knudsen, Mitigation of water fouling: technology status and challenges, Adv. Heat Tran. 31 (1998) 431–474, https://doi.org/10.1016/S0065-2717(08)70244-2.
[15] A.B. Alayande, J. Lim, J. Kim, S. Hong, A.S. Al-Amoudi, B. Park, Fouling control in SWRO desalination during harmful algal blooms: a historical review and future developments, Desalination 543 (2022) 116094, https://doi.org/10.1016/j.desal.2022.116094.
[16] S. Mikhaylin, L. Bazinet, Fouling on ion-exchange membranes: classification, characterization and strategies of prevention and control, Adv. Colloid Interf. Sci. 229 (2016) 34–56, https://doi.org/10.1016/j.cis.2015.12.006.
[17] L. Ni, Q. Shi, M. Wu, J. Ma, Y. Wang, Fouling behavior and mechanism of hydrophilic modified membrane in anammox membrane bioreactor: role of gel layer, J. Membr. Sci. 620 (2021) 118988, https://doi.org/10.1016/j.memsci.2020.118988.
[18] M. El Batouti, N.F. Alharby, M.M. Elewa, Review of new approaches for fouling mitigation in membrane separation processes in water treatment applications, Separations 9 (1) (2021) 1, https://doi.org/10.3390/separations9010001.
[19] T. Xiao, Z. Zhu, L. Li, J. Shi, Z. Li, X. Zuo, Membrane fouling and cleaning strategies in microfiltration/ultrafiltration and dynamic membrane, Sep. Purif. Technol. 318 (2023) 123977, https://doi.org/10.1016/j.seppur.2023.123977.
[20] A. Abdel-Karim, S. Leaper, C. Skuse, G. Zaragoza, M. Gryta, P. Gorgojo, Membrane cleaning and pretreatments in membrane distillation–a review, Chem. Eng. J. 422 (2021) 129696, https://doi.org/10.1016/j.cej.2021.129696.
[21] K. Katsoufidou, S. Yiantsios, A. Karabelas, Experimental study of ultrafiltration membrane fouling by sodium alginate and flux recovery by backwashing, J. Membr. Sci. 300 (1–2) (2007) 137–146, https://doi.org/10.1016/j.memsci.2007.05.017.
[22] B. Malczewska, J. Liu, M. Benjamin, Virtual elimination of MF and UF fouling by adsorptive pre-coat filtration, J. Membr. Sci. 479 (2015) 159–164, https://doi.org/10.1016/j.memsci.2015.01.032.
[23] S.M. Cabrera, L. Winnubst, H. Richter, I. Voigt, J. McCutcheon, A. Nijmeijer, Performance evaluation of an industrial ceramic nanofiltration unit for wastewater treatment in oil production, Water Res. 220 (2022) 118593, https://doi.org/10.1016/j.watres.2022.118593.
[24] F.C. Kramer, R. Shang, L.C. Rietveld, S.J.G. Heijman, Fouling control in ceramic nanofiltration membranes during municipal sewage treatment, Sep. Purif. Technol. 237 (2020), https://doi.org/10.1016/j.seppur.2019.116373.
[25] A. Al-Amoudi, R.W. Lovitt, Fouling strategies and the cleaning system of NF membranes and factors affecting cleaning efficiency, J. Membr. Sci. 303 (1–2) (2007) 4–28, https://doi.org/10.1016/j.memsci.2007.06.002.
[26] X. Cheng, W. Zhou, P. Li, Z. Ren, D. Wu, C. Luo, X. Tang, J. Wang, H. Liang, Improving ultrafiltration membrane performance with pre-deposited carbon nanotubes/nanofibers layers for drinking water treatment, Chemosphere 234 (2019) 545–557, https://doi.org/10.1016/j.chemosphere.2019.06.090.
[27] Y. Zhang, X. Wang, H. Jia, B. Fu, R. Xu, Q. Fu, Algal fouling and extracellular organic matter removal in powdered activated carbon-submerged hollow fiber

ultrafiltration membrane systems, Sci. Total Environ. 671 (2019) 351–361, https://doi.org/10.1016/j.scitotenv.2019.03.371.
[28] L. Li, C. Visvanathan, Membrane technology for surface water treatment: advancement from microfiltration to membrane bioreactor, Rev. Environ. Sci. Biotechnol. 16 (4) (2017) 737–760, https://doi.org/10.1007/s11157-017-9442-1.
[29] Y. Li, Y. Xu, L.C. Rietveld, S.G. Heijman, Calcium carbonate precoating/acid cleaning method for fouling control in ceramic nanofiltration membranes, Sep. Purif. Technol. (2024) 130002, https://doi.org/10.1016/j.seppur.2024.130002.
[30] I. Caltran, L. Rietveld, H. Shorney-Darby, S. Heijman, Separating NOM from salts in ion exchange brine with ceramic nanofiltration, Water Res. 179 (2020) 115894, https://doi.org/10.1016/j.watres.2020.115894.
[31] R. Shang, A. Goulas, C.Y. Tang, X. de Frias Serra, L.C. Rietveld, S.G. Heijman, Atmospheric pressure atomic layer deposition for tight ceramic nanofiltration membranes: synthesis and application in water purification, J. Membr. Sci. 528 (2017) 163–170, https://doi.org/10.1016/j.memsci.2017.01.023.
[32] B. Lin, S.G. Heijman, L.C. Rietveld, Catalytic pre-coat on ceramic nanofiltration membranes for segregation and Fenton cleaning of high-resistance colloids in direct surface water treatment, J. Membr. Sci. 694 (2024) 122401, https://doi.org/10.1016/j.memsci.2023.122401.
[33] A.J. Karabelas, D. Sioutopoulos, New insights into organic gel fouling of reverse osmosis desalination membranes, Desalination 368 (2015) 114–126, https://doi.org/10.1016/j.desal.2015.01.029.
[34] A.J. de Kerchove, M. Elimelech, Formation of polysaccharide gel layers in the presence of Ca2+ and K+ ions: measurements and mechanisms, Biomacromolecules 8 (1) (2007) 113–121, https://doi.org/10.1021/bm060670i.
[35] F.C. Kramer, R. Shang, S.G. Heijman, S.M. Scherrenberg, J.B. van Lier, L. C. Rietveld, Direct water reclamation from sewage using ceramic tight ultra-and nanofiltration, Sep. Purif. Technol. 147 (2015) 329–336, https://doi.org/10.1016/j.seppur.2015.04.008.
[36] K. Katsanou, H.K. Karapanagioti, Surface water and groundwater sources for drinking water, in: Applications of Advanced Oxidation Processes (AOPs) in Drinking Water Treatment, Springer, 2017, pp. 1–19, https://doi.org/10.1007/698_2017_140.
[37] M. Hashino, T. Katagiri, N. Kubota, Y. Ohmukai, T. Maruyama, H. Matsuyama, Effect of surface roughness of hollow fiber membranes with gear-shaped structure on membrane fouling by sodium alginate, J. Membr. Sci. 366 (1–2) (2011) 389–397, https://doi.org/10.1016/j.memsci.2010.10.025.
[38] Y. Ye, P. Le Clech, V. Chen, A. Fane, Evolution of fouling during crossflow filtration of model EPS solutions, J. Membr. Sci. 264 (1–2) (2005) 190–199, https://doi.org/10.1016/j.memsci.2005.04.040.
[39] E. Halewood, K. Opalk, L. Custals, M. Carey, D.A. Hansell, C.A. Carlson, Determination of dissolved organic carbon and total dissolved nitrogen in seawater using high temperature combustion analysis, Front. Mar. Sci. 9 (2022) 1061646, https://doi.org/10.3389/fmars.2022.1061646.
[40] Y.M. Moustafa, R.E. Morsi, Ion exchange chromatography-an overview, Column Chromatogr. 1 (2013) 1–30, https://doi.org/10.5772/55652.
[41] J. Jamadi-Torab, A. Malekzadeh, M. Rahbari-Sisakht, A.F. Ismail, State-of-the-art in forward osmosis membrane process: materials, fabrication, and applications, Chem. Eng. Process.-Process Intensification 216 (2025) 110385, https://doi.org/10.1016/j.cep.2025.110385.
[42] Y. Li, Y. Xu, L.C. Rietveld, S.G.J. Heijman, Calcium carbonate precoating/acid cleaning method for fouling control in ceramic nanofiltration membranes, Sep. Purif. Technol. 356 (2025) 130002, https://doi.org/10.1016/j.seppur.2024.130002.
[43] S.-J. Lee, J.-H. Kim, Differential natural organic matter fouling of ceramic versus polymeric ultrafiltration membranes, Water Res. 48 (2014) 43–51, https://doi.org/10.1016/j.watres.2013.08.038.
[44] A. Rahimpour, S. Madaeni, A. Taheri, Y. Mansourpanah, Coupling TiO2 nanoparticles with UV irradiation for modification of polyethersulfone ultrafiltration membranes, J. Membr. Sci. 313 (1–2) (2008) 158–169, https://doi.org/10.1016/j.memsci.2007.12.075.
[45] B.-C. Huang, Y.-F. Guan, W. Chen, H.-Q. Yu, Membrane fouling characteristics and mitigation in a coagulation-assisted microfiltration process for municipal wastewater pretreatment, Water Res. 123 (2017) 216–223, https://doi.org/10.1016/j.watres.2017.06.080.
[46] B.K. Dutta, Principles of Mass Transfer and Separation Processes, PHI Learning Pvt. Ltd, 2007, https://doi.org/10.1002/cjce.20228.
[47] R.W. Baker, Membrane Technology and Applications, John Wiley & Sons, 2023, https://doi.org/10.1002/9781118359686.
[48] R. Fagbenle, O.M. Amoo, A. Falana, S. Aliu, Applications of Heat, Mass and Fluid Boundary Layers, Woodhead Publishing Limited, 2020, https://doi.org/10.1016/C2018-0-01750-8.
[49] A. Imbrogno, M.N. Nguyen, A.I. Schäfer, Tutorial review of error evaluation in experimental water research at the example of membrane filtration, Chemosphere (2024) 141833, https://doi.org/10.1016/j.chemosphere.2024.141833.
[50] P.B. Stark, Before reproducibility must come preproducibility, Nature 557 (7706) (2018) 613–614, https://doi.org/10.1038/d41586-018-05256-0.
[51] S. Zhai, W. Zhang, T. Li, W. Zhang, L. Lv, B. Pan, Sodium hypochlorite assisted membrane cleaning: alterations in the characteristics of organic foulants and membrane permeability, Chemosphere 211 (2018) 139–148, https://doi.org/10.1016/j.chemosphere.2018.07.144.
[52] B. Matthews, A. Jones, N. Theodorou, A. Tudhope, Excitation-emission-matrix fluorescence spectroscopy applied to humic acid bands in coral reefs, Mar. Chem. 55 (3–4) (1996) 317–332, https://doi.org/10.1016/S0304-4203(96)00039-4.
[53] S.K. Panigrahi, A.K. Mishra, Inner filter effect in fluorescence spectroscopy: as a problem and as a solution, J. Photochem. Photobiol. C: Photochem. Rev. 41 (2019) 100318, https://doi.org/10.1016/j.jphotochemrev.2019.100318.
[54] R. Rai, R. Reddi, U. Rai, Developments and future directions of phase diagram, physicochemical and optical studies of binary organic complexes, Prog. Cryst. Growth Charact. Mater. 59 (2) (2013) 73–111, https://doi.org/10.1016/j.pcrysgrow.2013.04.001.
[55] S. Guo, Y. Wan, X. Chen, J. Luo, Loose nanofiltration membrane custom-tailored for resource recovery, Chem. Eng. J. 409 (2021) 127376, https://doi.org/10.1016/j.cej.2020.127376.
[56] M. Battestini Vives, J. Thuvander, A. Arkell, F. Lipnizki, Low-molecular-weight lignin recovery with nanofiltration in the kraft pulping process, Membranes **12** (3) (2022) 310, https://doi.org/10.3390/membranes12030310.
[57] A. Karar, F. Naamoune, A. Kahoul, Chemical and electrochemical study of the inhibition of calcium carbonate precipitation using citric acid and sodium citrate, Desalin. Water Treat. 57 (35) (2016) 16300–16309, https://doi.org/10.1080/19443994.2015.1077743.
[58] A.I. Mitsionis, T.C. Vaimakis, C.C. Trapalis, The effect of citric acid on the sintering of calcium phosphate bioceramics, Ceram. Int. 36 (2) (2010) 623–634, https://doi.org/10.1016/j.ceramint.2009.09.034.
[59] M. Ghoorah, B.Z. Dlugogorski, R.D. Balucan, E.M. Kennedy, Selection of acid for weak acid processing of wollastonite for mineralisation of CO2, Fuel 122 (2014) 277–286, https://doi.org/10.1016/j.fuel.2014.01.015.
[60] J. Tiwari, A. Ramanathan, K. Bauddh, J. Korstad, Humic substances: structure, function and benefits for agroecosystems—a review, Pedosphere 33 (2) (2023) 237–249, https://doi.org/10.1016/j.pedsph.2022.07.008.
[61] D. Chen, Y. Shen, W. Liu, Y. Xiao, Y. Li, Mechanisms of calcium carbonate scaling regulated by single and multi-ion interactions: insights from experiments and molecular dynamics simulations, J. Environ. Chem. Eng. 13 (5) (2025) 117723, https://doi.org/10.1016/j.jece.2025.117723.
[62] Y. Pan, T. Wang, H. Sun, W. Wang, Preparation and application of titanium dioxide dynamic membranes in microfiltration of oil-in-water emulsions, Sep. Purif. Technol. 89 (2012) 78–83, https://doi.org/10.1016/j.seppur.2012.01.010.
[63] M. Gou, Y. Zhao, B. Li, Y. Li, Z. Li, M. Wang, Scaling behavior of cation exchange membrane induced by Ca2+ during the electrodialysis for enriching lithium-containing solutions, J. Membr. Sci. 713 (2025) 123283, https://doi.org/10.1016/j.memsci.2024.123283.
[64] I.H. Ozofor, V.V. Tarabara, A.R. Da Costa, A.N. Morse, Analysis of microstructural properties of ultrafiltration cake layer during its early stage formation and growth, J. Membr. Sci. 620 (2021) 118903, https://doi.org/10.1016/j.memsci.2020.118903.
[65] S. Wang, Y. Li, K. Xiao, X. Huang, Fluorescence excitation-emission matrix as a novel indicator of assimilable organic carbon in wastewater: implication from a coal chemical wastewater study, Sci. Total Environ. 804 (2022) 150144, https://doi.org/10.1016/j.scitotenv.2021.150144.
[66] Y.-Q. Niu, J.-H. Liu, C. Aymonier, S. Fermani, D. Kralj, G. Falini, C.-H. Zhou, Calcium carbonate: controlled synthesis, surface functionalization, and nanostructured materials, Chem. Soc. Rev. 51 (18) (2022) 7883–7943, https://doi.org/10.1039/D1CS00519G.
[67] L. Upadhyaya, X. Qian, S. Ranil Wickramasinghe, Chemical modification of membrane surface—overview, Curr. Opin. Chem. Eng. 20 (2018) 13–18, https://doi.org/10.1016/j.coche.2018.01.002.
[68] M. Schulz, R.W. Smith, R.P. Sear, R. Brinkhuis, J.L. Keddie, Diffusiophoresis-driven stratification of polymers in colloidal films, ACS Macro Lett. 9 (9) (2020) 1286–1291, https://doi.org/10.1021/acsmacrolett.0c00363.
[69] M.A. Dheyab, A.A. Aziz, M.S. Jameel, O.A. Noqta, P.M. Khaniabadi, B. Mehrdel, Simple rapid stabilization method through citric acid modification for magnetite nanoparticles, Sci. Rep. 10 (1) (2020) 10793, https://doi.org/10.1038/s41598-020-67869-8.
[70] X. Yin, X. Li, Z. Hua, Y. Ren, The growth process of the cake layer and membrane fouling alleviation mechanism in a MBR assisted with the self-generated electric field, Water Res. 171 (2020) 115452, https://doi.org/10.1016/j.watres.2020.116045.
[71] J. Luo, Y. Wan, Mix-charged nanofiltration membrane: engineering charge spatial distribution for highly selective separation, Chem. Eng. J. 464 (2023) 142689, https://doi.org/10.1016/j.cej.2023.142689.
[72] Y.-l. Liu, X.-m. Wang, H.-w. Yang, Y.F. Xie, X. Huang, Preparation of nanofiltration membranes for high rejection of organic micropollutants and low rejection of divalent cations, J. Membr. Sci. 572 (2019) 152–160, https://doi.org/10.1016/j.memsci.2018.11.013.
[73] Z. Wang, J. Su, X. Hu, A. Ali, Z. Wu, Isolation of biosynthetic crystals by microbially induced calcium carbonate precipitation and their utilization for fluoride removal from groundwater, J. Hazard. Mater. 406 (2021) 124748, https://doi.org/10.1016/j.jhazmat.2020.124748.
[74] L. Zeng, T. Zhao, L. Wei, H. Jiang, M. Wu, Anion exchange membranes for aqueous acid-based redox flow batteries: current status and challenges, Appl. Energy 233 (2019) 622–643, https://doi.org/10.1016/j.apenergy.2018.10.063.
[75] T. Tong, A.F. Wallace, S. Zhao, Z. Wang, Mineral scaling in membrane desalination: mechanisms, mitigation strategies, and feasibility of scaling-resistant membranes, J. Membr. Sci. 579 (2019) 52–69, https://doi.org/10.1016/j.memsci.2019.02.049.
[76] Y.A. Tayeh, M.Y. Alazaiza, T.M. Alzghoul, M.J. Bashir, A comprehensive review of RO membrane fouling: mechanisms, categories, cleaning methods and

pretreatment technologies, J. Hazard. Mater. Adv. 18 (2025) 100684, https://doi.org/10.1016/j.hazadv.2025.100684.
[77] R. Reena, R. Sindhu, P.A. Balakumaran, A. Pandey, M.K. Awasthi, P. Binod, Insight into citric acid: a versatile organic acid, Fuel 327 (2022) 125181, https://doi.org/10.1016/j.fuel.2022.125181.
[78] M. Chen, D. Cao, B. Li, H. Pang, C. Zheng, Sodium citrate increases the aggregation capacity of calcium ions during microbial mineralization to accelerate the formation of calcium carbonate, Environ. Res. 224 (2023) 115479, https://doi.org/10.1016/j.envres.2023.115479.